The genomics of mimicry: Gene expression throughout development provides insights into convergent and divergent phenotypes in a Müllerian mimicry system

Mathieu Chouteau, Adam M M Stuckert, Melanie Mcclure, Troy M Lapolice, Tyler Linderoth, Rasmus Nielsen, Kyle Summers, Matthew D Macmanes

The genomics of mimicry: gene expression throughout development provides insights into convergent and divergent phenotypes in a Müllerian mimicry system

Running title: The genomics of mimicry

Adam M M Stuckert[1,2]*, Mathieu Chouteau[3], Melanie McClure[3], Troy M LaPolice[1], Tyler Linderoth[4], Rasmus Nielsen[4], Kyle Summers[2], Matthew D MacManes[1]

[1]Department of Molecular, Cellular, and Biomedical Sciences, University of New Hampshire

[2]Department of Biology, East Carolina University

[3]Laboratoire Écologie, Évolution, Interactions des Systèmes Amazoniens (LEEISA), Université de Guyane, CNRS, IFREMER, 97300 Cayenne, France

[4]Department of Integrative Biology, University of California, Berkeley

*corresponding author: stuckerta@gmail.com

Abstract:

A common goal in evolutionary biology is to discern the mechanisms that produce the astounding diversity of morphologies seen across the tree of life. Aposematic species, those with a conspicuous phenotype coupled with some form of defense, are excellent models to understand the link between vivid color pattern variations, the natural selection shaping it, and the underlying genetic mechanisms underpinning this variation. Mimicry systems in which multiple species share the same conspicuous phenotype can provide an even better model for understanding the mechanisms of color production in aposematic species, especially if comimics have divergent evolutionary histories. Here we investigate the genetic mechanisms by which vivid color and pattern are produced in a Müllerian mimicry complex of poison frogs. We did this by first assembling a high-quality de novo genome assembly for the mimic poison frog *Ranitomeya imitator.* This assembled genome is 6.8 Gbp in size, with a contig N50 of 300 Kbp and 93% of expected tetrapod genes. We then leveraged this genome to conduct gene expression analyses throughout development of four color morphs of *R. imitator* and two color morphs from both *R. fantastica* and *R. variabilis* which *R. imitator* mimics. We identified a large number of pigmentation and patterning genes that are differentially expressed throughout development, many of them related to melanocyte development, melanin synthesis, iridophore development, and guanine synthesis. Polytypic differences within species may be the result of differences in expression and/or timing of expression, whereas convergence for color pattern between species do not appear to be due to the same changes in gene expression. In addition, we identify the pteridine synthesis pathway (including genes such as *qdpr* and *xdh*) as a key driver of the variation in color between morphs of these species. Finally, we hypothesize that genes in the keratin family are important for producing different structural colors within these frogs.

Keywords:

Amphibians, aposematism, color pattern, color production, Dendrobatidae, Ranitomeya

Introduction:

The diversity of animal coloration in the natural world has long been a focus of investigation in evolutionary biology (Gray and McKinnon 2007; Beddard 1892; Longley 1917; Fox 1936). Color phenotypes can be profoundly shaped by natural selection, sexual selection, or both. Further, these color phenotypes are often under selection from multiple biotic (e.g. competition, predation) and abiotic (e.g. temperature, salinity) factors (Rudh and Qvarnström 2013). The mechanisms underlying color and pattern phenotypes are of general interest because they can help explain the occurrence of specific evolutionary patterns, particularly in systems where these phenotypes embody key adaptations driving biological diversification.

Adaptive radiations in aposematic species (those species which couple conspicuous phenotypes with a defense), provides examples of the effects of strong selection on such phenotypes (Sherratt 2008, 2006; Ruxton, Sherratt, and Speed 2004; Kang et al. 2017). In these biological systems, geographically heterogeneous predation produces rapid diversification of color and pattern within a species or group of species. This produces a diversity of polytypic phenotypes (defined as distinct defensive warning color signals in distinct localities) that are maintained geographically, with each population characterized by a unique phenotype that deters predators. This spatial mosaic of local adaptations maintained by the strong stabilizing selection exerted by predators also results in convergence of local warning signals in unrelated species. Examples of impressive diversification within species and mimetic convergence between species have been

documented in many biological systems, including *Heliconius* butterflies (Mallet and Barton 1989), velvet ants (Wilson et al. 2015), millipedes (Marek and Bond 2009), and poison frogs (Symula, Schulte, and Summers 2001; Stuckert, Venegas, and Summers 2014; Stuckert et al. 2014; Twomey et al. 2013), to name only a few of the documented examples of diverse aposematic phenotypes (Briolat et al. 2019).

Understanding the genomic architecture underpinning these diversification events has been of substantial importance to the field of evolutionary biology (Hodges and Derieg 2009). Hence, it is essential to examine these diverse color pattern phenotypes and determine the mechanisms by which both divergence and convergence occurs at the molecular level. The majority of our knowledge of the genomics of warning signals and mimicry comes from butterflies of the genus *Heliconius*. In these insects, a small number of key genetic loci of large phenotypic effect controls the totality of phenotypic variation observed within populations of the same species. These also provide the genetic underpinnings for mimetic convergence between distinct species (e.g., *WntA (Martin et al. 2012)* and *optix (Reed et al. 2011; Supple et al. 2013)*), though there are many others likely involved as well (Kronforst and Papa 2015). While *Heliconius* butterflies are excellent subjects for the study of mimicry, characterizing the genetics of mimicry in a phylogenetically distant system is critically important to determining whether adaptive radiations in warning signals and mimitic relationships are generally driven by a handful of key loci. Furthermore, given the dramatic differences in life history and social behavior between these clades, studying aposematism and mimicry in *Ranitomeya* is likely to provide general and important insights into convergent mimetic phenotypes and the evolutionary processes that produce them.

Here we investigate the genetics of convergent color phenotypes in *Ranitomeya* from Northern Peru. In this system, the mimic poison frog *(Ranitomeya imitator,* Dendrobatidae;

(Schulte 1986) underwent a rapid adaptive radiation, such that it mimics established congenerics (*R. fantastica, R. summersi*, and *R. variabilis*), thereby "sharing" the cost of educating predators—a classic example of Müllerian mimicry (Symula, Schulte, and Summers 2003, 2001; Stuckert, Venegas, and Summers 2014; Stuckert et al. 2014). This is a powerful system for the evolutionary study of color patterns, as the different *R. imitator* color morphs have undergone an adaptive radiation to converge on shared phenotypes with the species that *R. imitator* mimics.

Furthermore, despite the arrival of new genomic data that provides critical insights into the mechanisms of color production in amphibians in general (Burgon et al. 2020), and poison frogs in particular (Rodríguez et al. 2020; Twomey, Johnson, et al. 2020; Stuckert et al. 2019), our knowledge of amphibian genomics is critically behind that of other tetrapods, both in terms of genomic resources as well as in our ability to make inferences from these resources. This is largely due to the challenging nature of these genomes, most of which are extremely large (frog genomes range from 1-11Gb, with an interquartile range of 3-5Gb; Funk et al. 2018) and rich with repeat elements that have proliferated throughout the genome (Rogers et al. 2018). This makes many amphibians a nearly-intractable system for in-depth genomic analyses (Funk, Zamudio, and Crawford 2018; Rogers et al. 2018). As a result, there is a relative dearth of publicly-available amphibian genomes (14 anuran species as of September 1st, 2020). In fact, many of the available genomes are from a single group of frogs with a genome size of less than 1 Gbp, which is on the lower bound of known amphibian genome sizes (Funk, Zamudio, and Crawford 2018).

We investigated the genetics of Müllerian mimicry by first generating a high quality 6.8 Gbp *de novo* genome assembly for the mimic poison frog, *Ranitomeya imitator* (Figure 1). This is an important new resource for amphibian biologists, as it fills a substantial gap in the phylogenetic distribution of available amphibian genomes and enables for more detailed comparative work. A

comparison between our *R. imitator* genome and the *Oophaga pumilio* genome provides insights into genome evolution within the family Dendrobatidae, particularly the proliferation of repeat content. We highlight these results in this manuscript. We then utilized this high quality *Ranitomeya imitator* genome to examine gene expression patterns using RNA sequencing of skin tissue from early tadpole development all the way through to the end of metamorphosis in both the mimic (*R. imitator*) and model species (*R. fantastica* and *R. variabilis*). As such, we were able to keep track of patterns of expression in genes responsible for color throughout development both between color morphs, and between species. We aimed to identify the genes responsible for color patterning that are convergent between model and mimic, as well as those genes whose role in color and pattern may be species-specific or even population-specific. Color patterns within these species begin to appear early during development when individuals are still tadpoles, which is consistent with observations that chromatophores (the structural elements in the integument that contain pigments) develop from the neural crest early during embryonic development (DuShane 1935). This comparative genomic approach allowed us to carefully examine the genes and gene networks responsible for diversification of color patterns and mimicry in poison frogs.

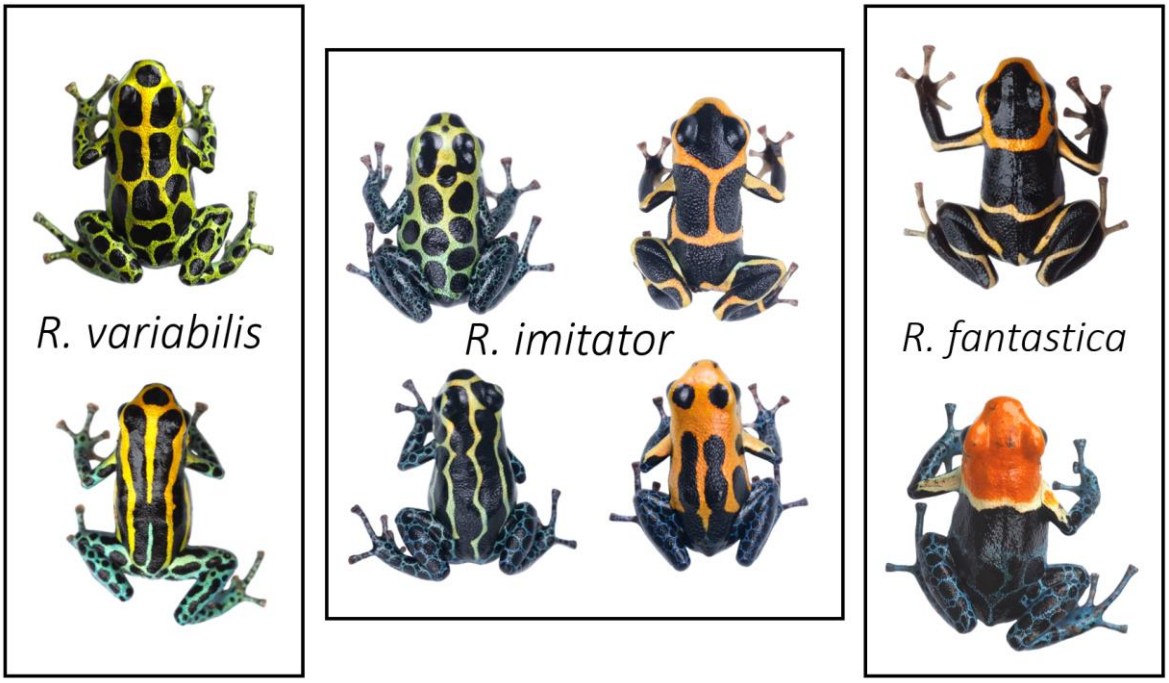

Figure 1. Normative photographs of frogs from the populations used in this study. The center box represents the four mimetic color morphs of *Ranitomeya imitator.* The left exterior box represents the two morphs of *R. variabilis* that *R. imitator* mimics, and the rightmost box represents two color morphs of *R. fantastica* that *R. imitator* has a convergent phenotype with. *R. imitator* photos by AS, *R. fantastica* and *R. variabilis* photos by MC.

Methods:

Permits:

R. imitator:

Animal use and research comply with East Carolina University's IACUC (AUP #D281) and the University of New Hampshire's IACUC (AUP #180705).

R. fantastica and *R. variabilis:*

The protocol for *R. fantastica* and *R. variabilis* sample collection was approved by the Peruvian Servicio Forestal y de Fauna Silvestre through the authorization number 232-2016-SERFOR/DGGSPFFS and export permit N° 17PE 001718 and the authorization from the French

Direction de l'Environnement, de l'Agriculture, de l'Alimentation et de la forêt en Guyane number 973-ND0073/SP2000116-13.

Data accessibility:

All read data, our *de novo* genome assembly, and our annotations are archived with the European Nucleotide Archive (accession number PRJEB28312; https://www.ebi.ac.uk/ena/browser/view/PRJEB28312). The genome assembly is available under assembly contig set CAJOBX010000000.1. Additional transcript evidence from unpublished studies as well as the gff file used in analyses are available in Stuckert et al. (2021). Code for assemblies, annotation, and all subsequent analyses are all available on GitHub (https://github.com/AdamStuckert/Ranitomeya_imitator_genome) and in Stuckert and LaPolice (2021).

Generating a *de novo* genome for *Ranitomeya imitator:*

Genome Sequencing Approach:

Because all sequencing technologies are known to be biased in both known and unknown ways, we utilized a variety of sequencing technologies to assemble this complex and large genome. At the time of genome construction, both sequencing technologies and assembly algorithms were undergoing rapid change, and as such the generation of an optimal assembly required substantial trial and error. For instance, several of the authors of this paper were involved in the strawberry poison frog genome assembly Rogers et al. 2018) and the difficulties encountered in the attempt to assemble that genome made it clear that short read data alone are insufficient if the goal is to assemble a highly-contiguous and complete genome. To overcome the limitations associated with

short read data, we collected linked and long read data from technologies thought to be complementary to one another (Illumina 10X, Oxford Nanopore, and Pacific Biosystems).

10X Chromium:

A single, likely male, subadult *R. imitator* of the 'intermedius' morph from the amphibian pet trade was used to produce a 10X library. This individual had no visible ovaries, and sex chromosomes in poison frogs are currently uncharacterized and therefore are not a mechanism used to identify sex. This frog was euthanized and high molecular weight DNA was extracted from liver tissue using the QIAGEN Blood & Cell Culture DNA Kit. 10X Genomics Chromium Genome library (Weisenfeld et al. 2017) was prepared by the DNA Technologies and Expression Analysis Cores at the University of California Davis Genome Center and sequenced on an Illumina HiSeq X by Novogene Corporation (Mudd et al. in prep).

Long read (Oxford Nanopore and Pacific BioSciences) sequencing:

Captive bred subadult frogs from the pet trade that originated from the region near Tarapoto, Peru (green-spotted morph, Figure 1) were euthanized and the skin and gastrointestinal tract was removed in order to reduce potential contamination from skin and gut microbial communities. To obtain the recommended mass of tissue for genomic DNA extraction, each frog was dissected into 8 approximately equal chunks of tissue from the remaining portions of the whole-body and DNA was extracted using a Qiagen Genomic Tip extraction kit. DNA concentration was quantified with a Qubit 3.0 and fragment length was assessed with a TapeStation using a D1000 kit.

For Nanopore sequencing we prepared libraries for direct sequencing via Oxford Nanopore using a LSK-109 kit. Samples were loaded onto either R9 or R10 flowcells, which yielded minimum throughput. We basecalled raw fast5 files from Nanopore sequencing using the "read_fast5_basecaller.py" script in the ONT Albacore Sequencing Pipeline Software version 2.3.4.

For Pacific Biosystems (PacBio) sequencing we used a Circulomics short-read eliminator (Circulomics Inc, Baltimore, MD, USA) kit to size select extracted DNA from 10 Kb progressively up to 25 Kb. After this, we sent ~15 µg of high molecular weight DNA to the Genomics Core Facility in the Icahn School of Medicine at Mt. Sinai (New York, USA) for library preparations and sequencing. Here libraries were prepared with 20-25 Kb inserts and were sequenced on three SMRTcell 8M cells on a Pacific Biosciences Sequel II.

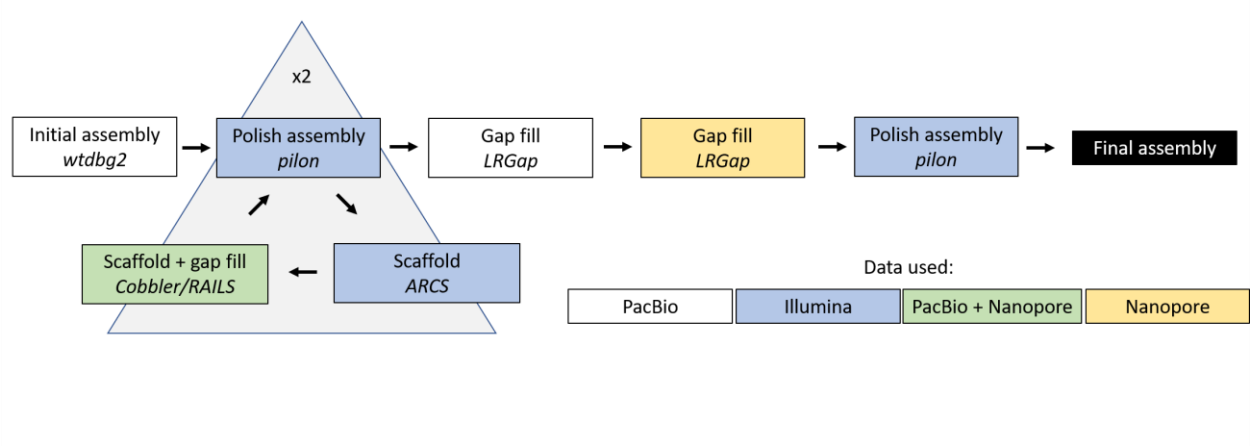

Figure 2. Flowchart of genome assembly approach. Colors of boxes represent the type of data used in that step (see internal legend) and italicized font indicate the program(s) used.

Genome assembly:

We took a multifaceted approach to constructing the *Ranitomeya imitator* genome, which contained iterative scaffolding steps. We detail our general approach here, and have a graphical depiction of this in Figure 2. PacBio has an algorithm to classify subreads that pass their minimum

quality expectations for subreads as "good" subreads, and all subsequent analyses used only those reads passing this threshold. We used the contig assembler wtdbg2 version 2.5 *(Ruan and Li 2019)* to create our initial assembly and create consensus contigs using only the PacBio data. Wtdbg2 uses a fuzzy *de bruijn* graph approach to assemble reads into contigs. Since PacBio reads have, on average, lower per-base accuracy than Illumina reads, we took several steps to correct individual bases in our assembly. To do this we first mapped the Illumina short reads to our assembly using BWA version 0.7.17-r1188 (H. Li and Durbin 2009). Polishing was then conducted using the software Pilon version 1.22 (Walker et al. 2014). We used a flank size of 5 bases (thus ignoring the last 5 well-aligned bases on either end of the alignment) and fixed both bases and gaps with a minimum size of 1 base.

We then used Arcs version 3.82 (Coombe et al. 2018) to scaffold our existing assembly using Illumina 10X data. Prior to doing this, we used the "basic" function within the program Longranger (Marks et al. 2019) to trim, error correct, and to identify barcodes in the 10X data. We then used the "arks.mk" makefile provided in the Arcs GitHub page (https://github.com/bcgsc/arcs/blob/master/Examples/arcs-make), to run the Arcs software. This makefile aligns the barcoded 10X data from Longranger using BWA, then runs Arcs to scaffold our assembly. After scaffolding our assembly with the 10X data, we ran one round of Cobbler version v0.6.1 (Warren 2016) to gap-fill regions of unknown nucleotides (depicted as "N"s) in our assembly. Our input data was the full set of our PacBio and Nanopore data, which was mapped to our assembly using minimap2 version 2.10-r761 (Heng Li 2018) with no preset for sequencing platform. We then ran RAILS version 5.26.1 (Warren 2016) to scaffold again, with the same input data as for Cobbler. We aligned the long-read data with Minimap2 because it maps a higher proportion of long reads than other aligners and we used BWA because it is more accurate for

short-read data (Heng Li 2018). After this we polished our assembly again by mapping Illumina reads with BWA and Pilon. We then attempted to fill in gaps within our assembly using LR Gapcloser (Xu et al. 2019). We ran this program iteratively, first using the Nanopore data and specifying the "-s n" flag. We then filled gaps using LR Gapcloser with PacBio reads and the "-s p" flag. Following this, we again polished our assembly using BWA and Pilon.

We examined genome quality in two main ways. First we examined the presence of genic content in our genome using Benchmarking Universal Single-Copy Orthologs version 3.0.0 (BUSCO; (Simão et al. 2015) using the tetrapod database (tetrapoda_odb9; 2016-02-13). BUSCO version 4.0 was released during this project, so we also examined our final assembly with BUSCO version 4.0.6 and the tetrapod database (tetrapoda_odb10; 2019-11-20). Our second method of genome examination was genome contiguity. We used the assemblathon perl script (https://github.com/KorfLab/Assemblathon/blob/master/assemblathon_stats.pl) to calculate overall numbers of scaffolds and contigs as well as contiguity metrics such as N50 for both.

Repeats and genome annotation:

We modeled genomic repeats with Repeat Modeler version 1.0.8 (Smit and Hubley 2008-2015) using RepBase database 20170127. We used the classified consensus output from Repat Modeler as input to Repeat Masker version 4.1.0 (Smit, Hubley, and Green 2013-2015) with the *Homo sapiens* database specified. We used a combined database of Dfam_3.1 and RepBase-20181026 (Bao, Kojima, and Kohany 2015).

We annotated our genome using Maker version 3.01.02 (Campbell et al. 2014). We used transcript evidence from *R. imitator* to aid in assembly ("est2genome=1"). We produced transcript evidence from gene expression data of various *R. imitator* tissues and populations; for additional

248 details on transcript evidence used to annotate this genome please see the Appendix. We
249 annotated the genome using both the draft genome as well as a repeat masked genome from
250 Repeat Modeler and Repeat Masker in order to identify the best annotation of our genome.
251 We used BUSCO version 4.0.6 (Simao *et al.* 2015) on the final version of the *R. imitator*
252 genome to locate putative duplicated orthologs within the genome. BUSCO searches a database of
253 universal single copy orthologs to measure genic completeness of the genome. BUSCO identifies
254 whether these single copy orthologs are present in the genome and if they are complete or
255 fragmented. Additionally, it identifies whether these orthologs are present in a single copy or
256 duplicated in the genome. Given the high proportion of duplicated orthologs present in our
257 genome, we proceeded to investigate the read support for each of these duplicated regions across
258 our sequencing technologies. We aligned PacBio data using Minimap2 version 2.10 (Heng Li 2018).
259 After we aligned the data, we used SAMtools version 1.10 (Heng Li et al. 2009) to generate the
260 depth at each base in the genome for data from each sequencing platform. We wrote a custom
261 Python script (see code availability statement for link to code repository) to extract the depth per
262 base within the duplicated regions of the genome. Additionally, we extracted the genic regions
263 identified as single copy genes by BUSCO in the same fashion. This allowed us to examine if there
264 were any discrepancies between the duplicates and the rest of the genomic sequence. For each
265 region in both the single copy and duplicated genes we calculated mean and standard deviation.
266 We identified regions that were outliers in sequencing depth by identifying genes that had average
267 sequencing depth that was outside of the average genome-wide sequencing depth plus two
268 standard deviations, or below 10x coverage. We did this because average coverage varied
269 dramatically at a per-base scale (PacBio genome wide coverage: average = 34.5 ± 79.1 sd). We view

this as a method of detecting duplicated regions that have plausibly been incorrectly assembled (i.e., spuriously collapsed or duplicated), and is not completely definitive.

IDENTIFICATION OF COLOR PATTERN CANDIDATE GENES

Gene expression sample preparation:

Samples were prepared differently for the mimic (*R. imitator*) and the model species (*R. fantastica* and *R. variabilis*). During the course of our work, we discovered that there were multiple groups approaching the same questions using collected samples from different species, but at slightly different timepoints. In light of this, we chose to combine our efforts into a single manuscript in an attempt at making broader inferences. We acknowledge this, and as a result, the data in this manuscript are analyzed in a manner concordant with these differences.

Ranitomeya imitator:

The initial breeding stock of *Ranitomeya imitator* was purchased from Understory Enterprises, LLC (Chatham, Canada). Frogs used in this project represent captive-bred individuals sourced from the following wild populations going clockwise from top left in Figure 1: Tarapoto (green-spotted), Sauce (orange-banded), Varadero (redheaded), and Baja Huallaga (yellow-striped). Tadpoles were sacrificed for analyses at 2, 4, 7, and 8 weeks of age. We sequenced RNA from a minimum of three individuals at each time point from the Sauce, Tarapoto, and Varadero populations (except for Tarapoto at 8 weeks), and two individuals per time point from the Huallaga population. Individuals within the same time points were sampled from different family groups (Appendix Table 1).

Tadpoles were anesthetized with 20% benzocaine (Orajel), then sacrificed via pithing. Whole skin was removed and stored in RNA later (Ambion) at -20°C until RNA extraction. Whole skin was lysed using a BeadBug (Benchmark Scientific, Sayreville, NJ, USA), and RNA was then extracted using a standardized Trizol protocol. RNA was extracted from the whole skin using a standardized Trizol protocol, cleaned with DNAse and RNAsin, and purified using a Qiagen RNEasy mini kit. RNA Libraries were prepared using standard poly-A tail purification with Illumina primers, and individually barcoded using a New England Biolabs Ultra Directional kit as per the manufacturer's protocol. Individually barcoded samples were pooled and sequenced using 50 bp paired end reads on three lanes of the Illumina HiSeq 2500 at the New York Genome Center.

Ranitomeya fantastica and *Ranitomeya variabilis*:

We set up a captive colony in Peru (see Appendix) consisting of between 6 and 10 wild collected individuals per locality. We raised the tadpoles on a diet consisting of a 50/50 mix of powdered spirulina and nettle, which they received 5 times a week. Tadpoles were raised individually in 21oz plastic containers, within outside insectaries covered with 50% shading cloth, and water change was performed with rainwater. Three tadpoles per stage (1, 2, 5, 7, and 8 weeks after hatching; see Appendix Table 1) were fixed in an RNAlater (Ambion) solution. To do so, tadpoles were first euthanized in a 250 mg/L benzocaine hydrochloride bath, then rinsed with distilled water before the whole tadpole was placed in RNAlater and stored at 4°C for 6h before being frozen at -20°C for long-term storage. Before RNA extraction, tadpoles were removed from RNA later and the skin was dissected off. Whole skin was lysed using a Bead Bug, and RNA was then extracted using a standardized Trizol protocol. RNA libraries were prepared using standard poly-A tail purification, prepared using Illumina primers, and individually dual-barcoded using a New

England Biolabs Ultra Directional kit. Individually barcoded samples were pooled and sequenced on four lanes of an Illumina HiSeq X at NovoGene (California, USA). Reads were paired end and 150 base pairs in length.

Differential gene expression:

We indexed our new *Ranitomeya imitator* genome using STAR version 2.5.4a (Dobin et al. 2013). We removed adaptor sequences from reads using Trimmomatic version 0.39 (Bolger, Lohse, and Usadel 2014). We then aligned our trimmed reads to our genome using STAR version 2.5.4a (Dobin et al. 2013), allowing 10 base mismatches (--outFilterMismatchNmax 10), a maximum of 20 multiple alignments per read (--outFilterMultimapNmax 20), and discarding reads that mapped at less than 50% of the read length (--outFilterScoreMinOverLread 0.5). We then counted aligned reads using htseq-count version 0.11.3 (Anders, Pyl, and Huber 2015).

Differential expression analyses were conducted in R version 3.6.0 (Team 2019) using the package DESeq2 (Love, Anders, and Huber 2014). Some genes in our annotated genome are represented multiple times, and thus the alignment is nearly to gene level with some exceptions. As a result, when we imported data into R we corrected for this by merging counts from htseq-count into a gene-level count. We filtered out low expression genes by removing any gene with a total experiment-wide expression level ≤ 50 total counts. cDNA libraries for *R. imitator* were sequenced at a different core facility than those of *R. fantastica* and *R. variabilis*, so in order to statistically account for batch effects we analyzed the data from each species independently (combining all species and batch effects in our dataset produces rank deficient models). For each species we compared two models using Likelihood Ratio Tests, one which tested the effect of color morph and the other which tested the effect of developmental stage. Both models included sequencing lane,

developmental stage, and color morph as fixed effects. We used a Benjamini and Hochberg (Benjamini and Hochberg 1995) correction for multiple comparisons and used an alpha value of 0.01 for significance. We then extracted data from our models for particular *a priori* color genes that play a role in color or pattern production in other taxa. This *a priori* list was originally used in Stuckert et al. (Stuckert et al. 2019), but was updated by searching for genes that have been implicated in coloration in genomics studies from the last three years. Plots in this manuscript were produced using ggplot2 (Wickham 2011).

Finally, we ran an analysis with the specific intent of identifying genes involved in the production of different color morphs that are convergent between model (*R. fantastica* or *R. variabilis*) and mimic (*R. imitator*). To do this we conducted a Walds test within species between the spotted and striped morph of *R. imitator* and *R. variabilis* that incorporated sequencing lane, tadpole age, and color morph as fixed effects. We then identified the set of genes that are differentially expressed between color morphs in both species, as well as those that showed species-specific patterns. We did this same within species comparison using the banded and redheaded morphs of *R. imitator* and *R. fantastica*. In order to further elucidate potential genes that may influence convergent and divergent phenotypes in multiple species, we examined the list of all differentially expressed genes between color morphs in *R. imitator* (via the Likelihood Ratio Test described above) for genes that are differentially expressed between color morphs in *R. fantastica* or *R. variabilis* (via the Walds tests we conducted).

Weighted Gene Correlation Network Analysis:

To identify networks of genes that interact in response to differences in color morphs, species, or developmental stage, we used weighted gene co-expression network analysis (WGCNA),

an approach used for finding clusters of transcripts with highly correlated expression levels and for relating them to phenotypic traits, using the package WGCNA (Langfelder and Horvath 2008). Although WGCNA names modules after colors, these name designations are unrelated to any phenotype in our data. For the WGCNA analysis, we used the variance stabilizing transformed data produced by DESeq2 at this stage. WGCNA requires filtering out genes with low expression, which we did prior to all differential expression analyses. We estimated a soft threshold power (β) that fits our data, by plotting this value against Mean Connectivity to determine the minimum value at which Mean Connectivity asymptotes, which represents scale free topology. For our data, we used $\beta = 10$, the recommended minimum module size of 30, and we merged modules with a dissimilarity threshold below 0.25. We then tested whether the eigenmodules (conceptually equivalent to a first principal component of the modules) were correlated with color morphs, species, or developmental stage at $p < 0.05$. While there may be many modules of co-expressed genes, only a few are correlated with any given phenotype; these are the modules of particular interest to us. To examine gene ontology of these modules we then took module membership for each gene within these modules and ranked them in decreasing order of module membership. We then supplied this single ranked list of module membership to the Gene Ontology enRIchment anaLysis and visuaLizAtion tool (GOrilla), and ran it in fast mode using *Homo sapiens* set as the organism (Eden et al. 2009).

Results:

Ranitomeya imitator Genome:

Genome assembly:

Our initial contig assembly was 6.77 Gbp in length, had a contig N50 of 198,779 bp, and contained 92.3% of expected tetrapod core genes after polishing with Pilon. After this initial assembly, we conducted two rounds of scaffolding and gap-filling our genome using our data. Our final genome assembly was 6.79 Gbp in length and consisted of 73,158 scaffolds ranging from 1,019-59,494,618 bp in length with a scaffold N50 of 397,629 bp (77,639 total contigs with an N50 of 301,327 bp, ranging from 1,019-59,494,618 bp; see Figure 3). A total of 8,149 contigs were placed into scaffolds by our iterative scaffolding and gap-filling, and on average scaffolds contain 1.1 contigs. Based on our BUSCO analysis, the final genome contained 93.0% of expected tetrapod genes. We assembled 69.8% single copy orthologs and 23.2% duplicated orthologs. An additional 1.8% were fragmented and 5.2% were missing (see Supplemental Table 1). The predicted transcriptome from Maker had 79.1% of expected orthologs, 59.4% of which were single copy and complete, 19.7% of which were duplicated, 7.5% of which were fragmented, and 13.4% missing.

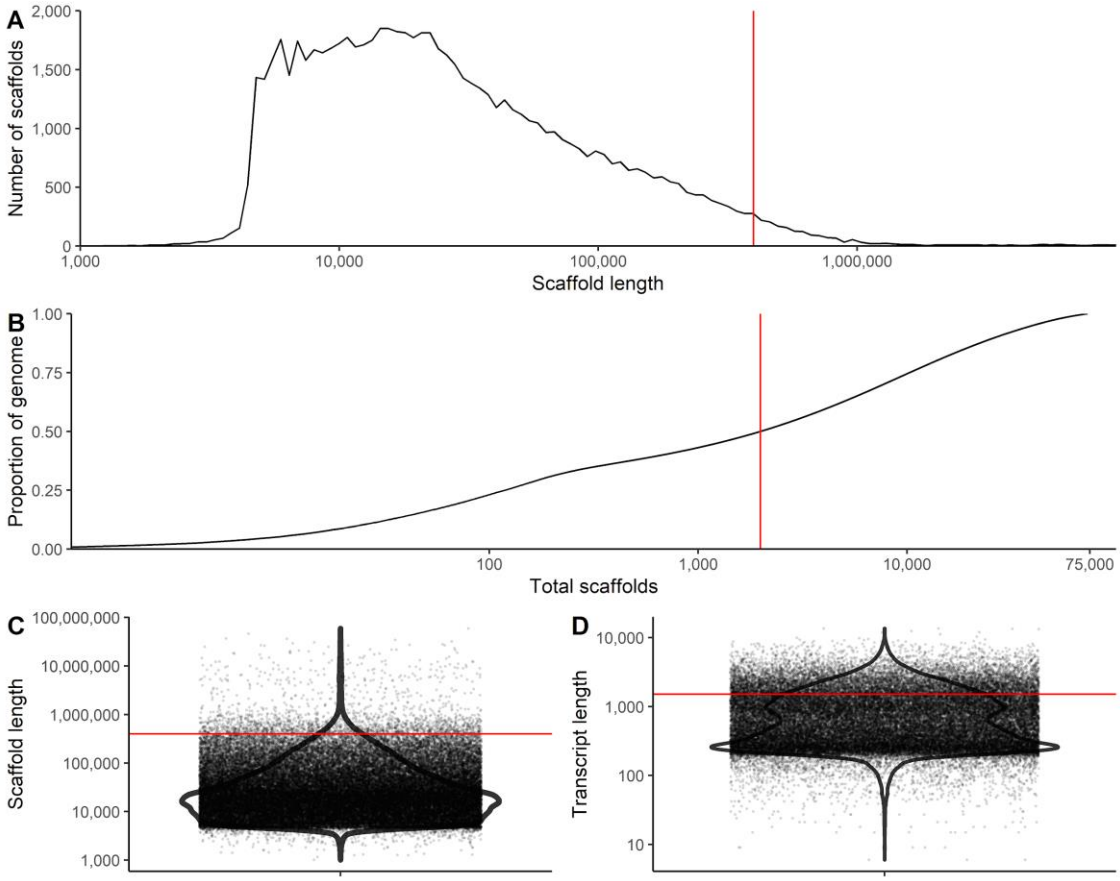

Figure 3. Summary figures of genome assembly. A) Distribution of scaffolds by length. B) The cumulative proportion of the genome represented by scaffolds. Scaffolds were ordered from longest to shortest prior to plotting, therefore in this panel the longest scaffolds are represented in the left portion of the figure. C) Violin plot of the distribution of scaffold lengths in the genome. D) Violin plot of the length of transcripts in the genome as predicted by Maker. Red lines represent N50 in A, C, and D and L50 in B.

Repetitive *elements:*

Our analyses indicate a high proportion of repeats in the *R. imitator* genome (see Figure 4). Repeat Modeler masked 54.14% of total bases in the genome, of which 50.3% consisted of repeat elements (see Table 1). Repeat masker was unable to classify most of the masked repeat bases (1.7 Gbp representing 25.67% of the genome). Many of the remaining repeats were retroelements (18.36%), nearly 10% of which were LINEs. Just under 8.5% were LTR elements, including 7.45%

GYPSY/DIRS1 repeats. Given the quality of repeat databases and the scarcity of amphibian genomic resources in these databases, our results likely represent an underrepresentation of repeats in the genome as a whole. A fairly large proportion of the genome's repeat elements are likely to be unassembled and missing in the genome, contributing to our underestimation of repeat content. Additionally, many of these repeat classes were long repeats (see Figure 5). For example, the average length of repeats was > 1000 bp in L1 (1093.4 ± 1490.5), L1-Tx1 (1417.3 ± 1372.3), Gypsy (1349.0 ± 1619.3), and Pao (1254.9 ± 1385.8) repeat elements. Summary statistics on the number of instances, range, average length, and standard deviation of range can be found in Supplemental Table 2.

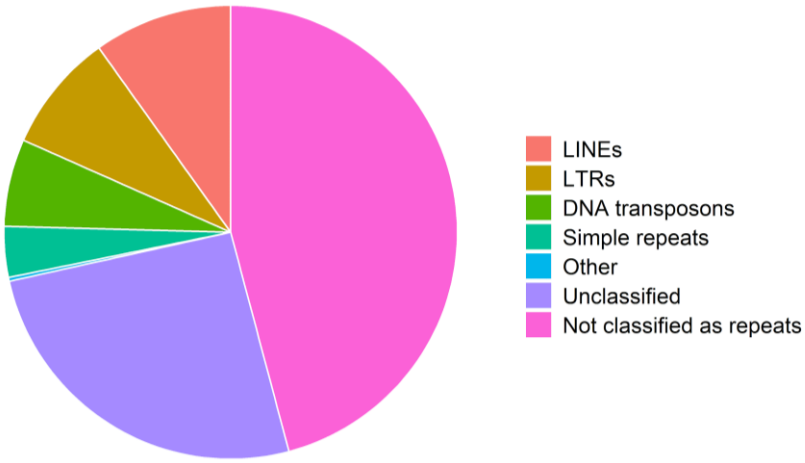

Figure 4. Pie chart of the contents of the *Ranitomeya imitator* genome. Much of the genome is classified as repeat elements, although we were unable to identify many of those.

Element type			Number of elements	Total length of elements (bp)	Percentage of genomic sequence
Retroelements			1108460	1247087328	18.36
	SINEs		5440	428468	0.01
	Penelope		60001	32685796	0.48
	LINEs		655737	671087603	9.88
		CRE/SLACS	0	0	0
		L2/CR1/Rex	241795	194226476	2.86
		R1/LOA/Jockey	0	0	0
		R2/R4/NeSL	1089	644862	0.01
		RTE/Bov-B	8249	5177385	0.08
		L1/CIN4	343520	436013718	6.42
	LTR elements		447283	575571257	8.47
		BEL/Pao	3504	2966778	0.04
		Gypsy/DIRS1	340203	505961953	7.45
		Retroviral	85837	44644563	0.66
DNA transposons			703907	423320187	6.23
	hobo-Activator		144891	93261380	1.37
	Tc1-IS630-Pogo		504231	296915689	4.37
	En-Spm		0	0	0
	MuDR-IS905		0	0	0
	PiggyBac		10239	8260072	0.12
	Tourist/Harbinger		19834	14807248	0.22
	Other (Mirage, P-element, Transib)		0	0	0
Rolling-circles			4811	2310034	0.03
Unclassified			5605837	1743383014	25.67
Total interspersed repeats				3413790529	50.26
Small RNA			0	0	0
Satellites			0	0	0
Simple repeats			1930599	246155996	3.62
Low complexity			211720	14981007	0.22

Table 1. Repeat elements classified by Repeat Masker. Most repeats fragmented by insertions or deletions were counted as a single element.

A large proportion of tetrapod orthologs (i.e., those genes in BUSCO's tetrapoda database) are present in duplicate copies that are spread throughout scaffolds in the genome (23.2%). On average, scaffolds had 1.92 ± 2.93 duplicated orthologs, with a median and mode of 1. When normalized per 10,000 bp, the average was 0.060 ± 0.108 SD duplicated orthologs per 10,000 bp of

a scaffold, with a median of 0.032. Intriguingly, the majority of orthologs identified as single copies by BUSCO had average coverage greater than the average genome-wide coverage. Duplicated orthologs, on the other hand, had coverage lower than the average genome-wide coverage. Single copy orthologs had an average coverage of 60.5 ± 29.3 SD, whereas duplicated orthologs had an average coverage of 41.6 ± 31.1 SD, and a two-tailed student t-test revealed a significant difference in coverage between single and duplicate copy orthologs (t_{5094} = 23.965, p-value < 0.0001; See Supplemental Figure 1).

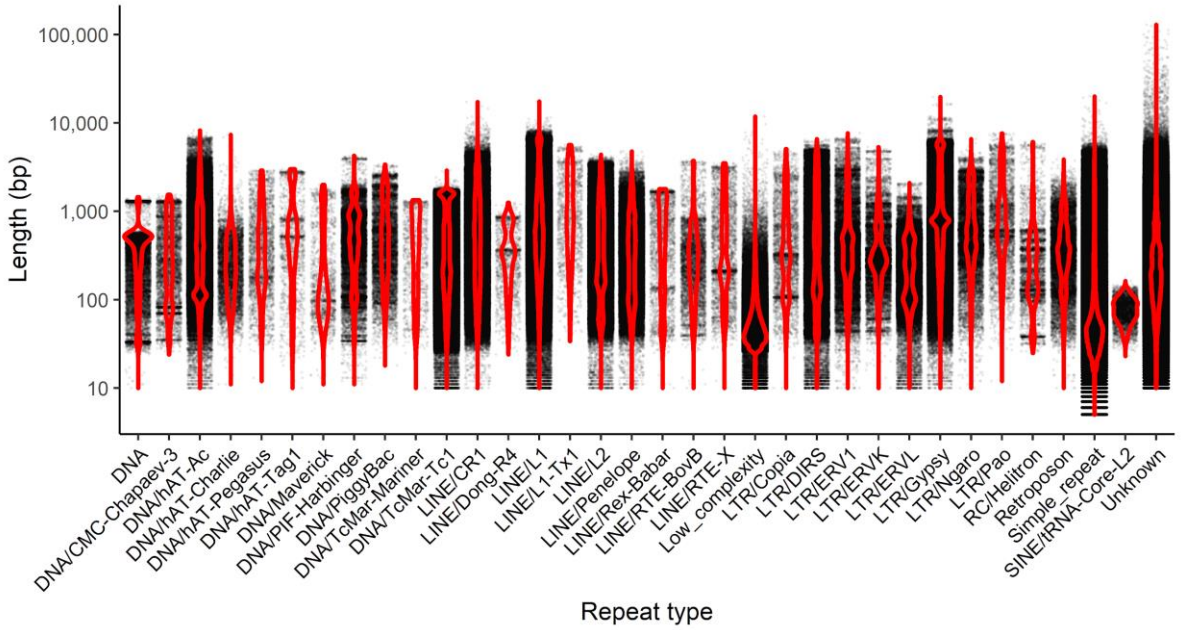

Figure 5. A violin plot of the length of individual repeats in the *R. imitator* genome. Each point represents a single instance of the repeat.

Gene expression:

We aligned an average of 20.97 million reads (± 6.7 sd) per sample. On average, 73.27% of reads were uniquely mapped (± 4.75% sd). Mapping rates were slightly higher in *R. imitator* than in *R. fantastica* or *R. variabilis*, because the libraries were of slightly higher quality in *R. imitator.* To further test if this was an artifact derived from mapping reads from other species to the *R. imitator*

genome, we also mapped these reads to species-specific transcriptome assemblies. We assembled these using data for each species in this study using the Oyster River Protocol (MacManes 2017); additional details on this protocol can be found in the appendix. After mapping our read data to these species-specific transcriptome assemblies we found similar results to that of our genome-guided mapping. Thus, our mapping rates are driven primarily by the slightly lower quality of the *R. fantastica* and *R. variabilis* cDNA libraries (as exhibited by slightly lower Phred scores towards the 3' end of reads) and not by species-specific differences in coding regions. For data on number of reads and mapping rates in each sample please see (Supplemental Table 3). All gene expression count data can be found in the GitHub repository (https://github.com/AdamStuckert/Ranitomeya_imitator_genome/tree/master/GeneExpression/data). Patterns of gene expression are largely driven by developmental stage (principal component 1; 43% of variation) and species (principal component 2; 13% of variance; see Figure 6). We note that differences in sample preparation and sequencing localities between *R. imitator and R. fantastica/variabilis* may be driving a portion of the pattern in principal component 2. However, the pattern found in principal component 2 closely parallels phylogeny, as *R. fantastica* and *R. variabilis* are more closely related to each other than either are to *R. imitator* (Brown et al. 2011). We then conducted a test for the effect of color morph and developmental stage for each species independently. For a list of all differentially expressed color genes see Supplemental Table 4. For a list of all differentially expressed genes at alpha < 0.01 and alpha < 0.05 see Supplemental Table 5 and 6 respectively.

Between developmental stage comparisons:

In our comparison of developmental stages we found many differentially expressed genes (q value < 0.01) in each species (*R. imitator* = 2,039, *R. fantastica* = 2,247, *R. variabilis* = 2,734; Table 2). Most of these are unlikely to be related to color and patterning, although a small fraction of differentially expressed genes (average 3.5%) are found in our *a priori* list of genes that influence the generation of color or patterning in other taxa (*R. imitator* = 92, *R. fantastica* = 106, *R. variabilis* = 77). Amongst genes that were significantly differentially expressed between developmental stages we identified genes related to carotenoid metabolism (e.g., *bco1, retsat, scarb2, ttc39b;* Figure 7), the synthesis of pteridines (e.g., *gchfr, qdpr, pts, xdh;* Figure 7), genes related to melanophore development and melanin synthesis (*dct, kit, lef1, mitf, mlph, mreg, notch1, notch2, sfxn1, sox9, sox10, tyr*, and *tyrp1;* Figure 8), genes putatively related to the production of iridophores and their guanine platelets (e.g., *gart, gas1, paics, pacx2, pax3-a, pnp, rab27a, rab27b, rab7a, rabggta;* Figure 9), and genes related to patterning (*notch1, notch2*).

Between morph comparisons:

In our comparison of color morph we found many significantly differentially expressed genes in each species (*R. imitator* = 1,528, *R. fantastica* = 1,112, *R. variabilis* = 1,065; Table 2). Most of these are unlikely to be related to color and patterning, although a small fraction of differentially expressed genes (average 3.3%) are related to the generation of color or patterning in other taxa (*R. imitator* = 39, *R. fantastica* = 46, *R. variabilis* = 33). Amongst genes that were differentially expressed between color morphs we identified genes related to carotenoid metabolism or xanthophore production (e.g., *aldh1a1, ttc39b;* Figure 7), the synthesis of pteridines (e.g., *gchfr, qdpr, pts, xdh;* Figure 7), genes related to melanophore development and melanin synthesis (*kit, lef1, mlph, mreg, sfxn1, sox9, sox10*), and genes putatively related to the production of iridophores

and their guanine platelets (e.g., *atic, dock7, gart, paics, pacx2, pax3-a, rab27a, rab27b, rab7a, rabggta;* Figure 9).

Species	LRT between morphs		LRT between developmental stages		Genes differentially expressed between color morphs and developmental stages
	Differentially expressed genes	Differentially expressed genes *a priori color genes*	Differentially expressed genes	Differentially expressed genes *a priori color genes*	
R. imitator	1,528	39	2,039	92	249
R. fantastica	1,112	46	2,247	106	407
R. variabilis	1,065	33	2,734	77	574

Table 2. Number of differentially expressed genes for each comparison. LRT = likelihood ratio test.

Convergent gene expression patterns between model and mimic:

We compared gene expression between morphs for which we could make a direct comparison of expression between model and mimic (i.e., striped vs spotted, banded vs redheaded). In the striped vs spotted comparison, we identified 323 differentially expressed genes in *R. imitator* and 1,260 in *R. variabilis*. Of these genes, 47 were shared between the two species and one was in our a priori color gene list (*edaradd*). In the banded vs redheaded comparison, we identified 1,035 differentially expressed genes in *R. imitator* and 1,335 in *R. fantastica*. Of these genes, 128 were shared between the two species and two were in our a priori color gene list (*pkc-3* and *qdpr*). We additionally broadened our search out a bit further to examine any gene differentially expressed between morphs in two or more of our analyzed species. Using this

511 method, we identified an additional 10 color genes (*crabp2, dst, edar, erbb3, gchfr, kitlg, krt2,*

512 *rab27b, rb1,* and *tspan36*).

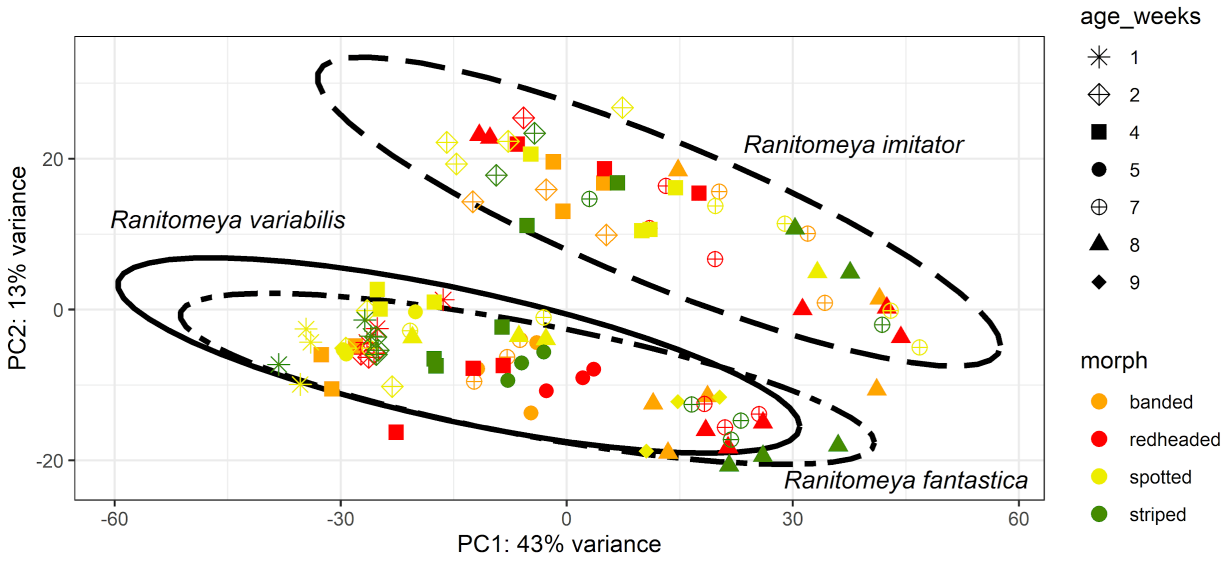

513

514 Figure 6. Principal component analysis of gene expression. The axes are labeled with the proportion
515 of the data explained by principal components 1 and 2.
516

517
518

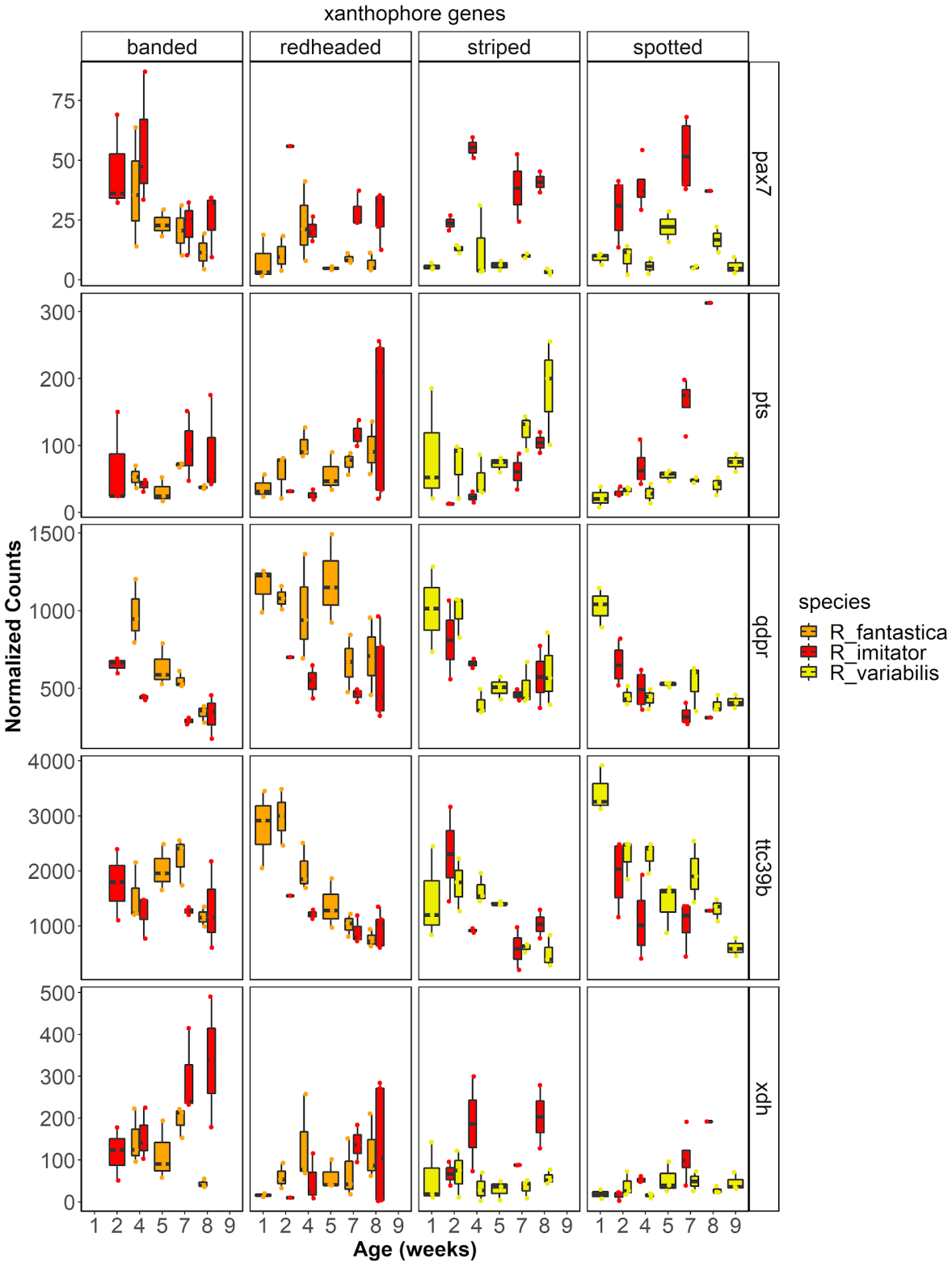

519

520 Figure 7. Gene expression for select carotenoid and pteridine genes.

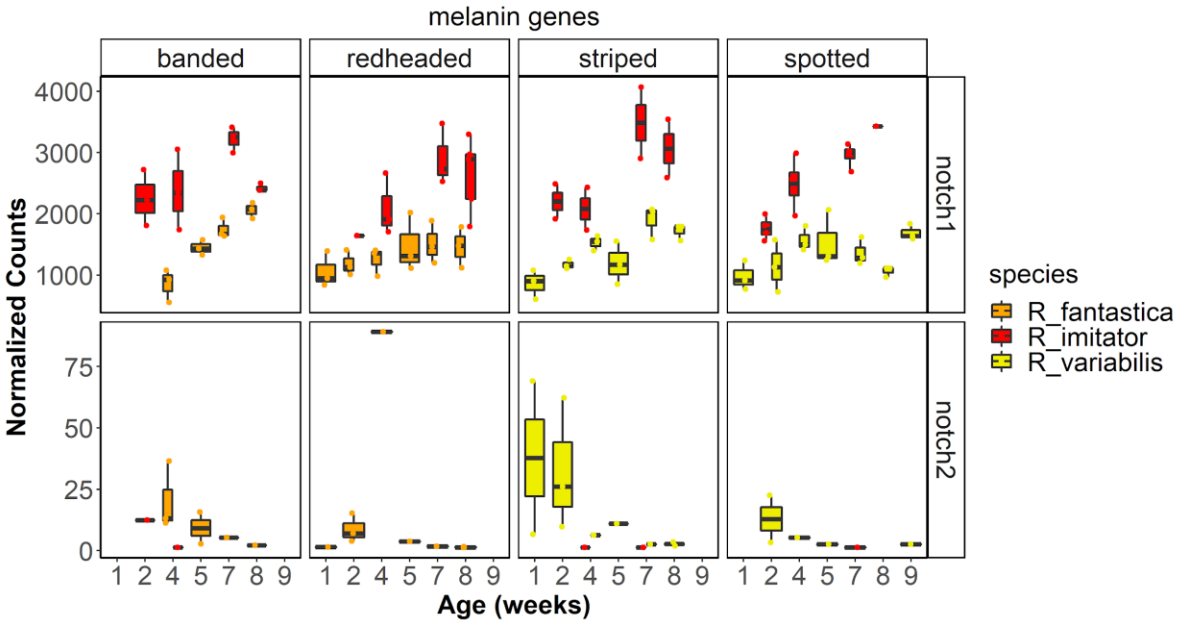

Figure 8. Gene expression for select melanin genes.

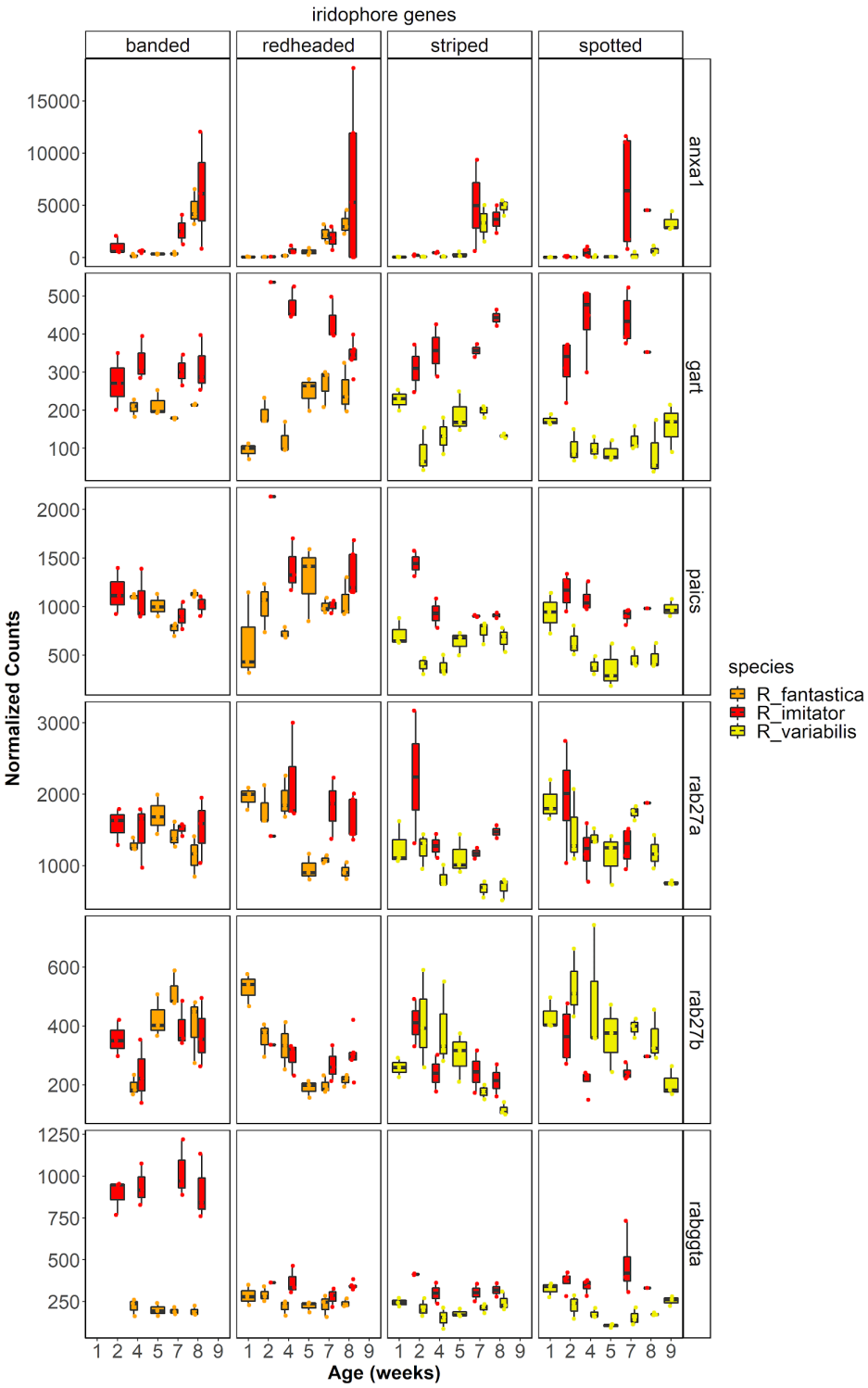

Figure 9. Gene expression for select iridophore genes.

Weighted Gene Correlation Network Analysis:

We identified 20 individual gene modules in our expression data using WGCNA (see Figure 10 WGCNA modules). Of these, we identified 14 modules that were significantly correlated with developmental stage; green ($r = -0.330$; $p < 0.0001$), midnight blue ($r = -0.446$; $p < 0.0001$), purple ($r = -0.442$; $p < 0.0001$), greenyellow ($r = -0.652$; $p < 0.0001$), light cyan ($r = -0.510$; $p < 0.0001$), black ($r = -0.268$; $p = 0.0040$), grey 60 ($r = -0.405$; $p < 0.0001$), red ($r = -0.585$; $p < 0.0001$), light green ($r = 0.573$; $p < 0.0001$), blue ($r = 0.669$; $p < 0.0001$), cyan ($r = 0.734$; $p < 0.0001$), magenta ($r = 0.215$; $p = 0.022$), light yellow ($r = -0.345$; $p = 0.00017$), and salmon ($r = 0.431$; $p < 0.0001$). We identified 10 modules that were significantly correlated with species; green ($r = -0.280$; $p = 0.0025$), pink ($r = -0.566$; $p < 0.0001$), purple ($r = 0.308$; $p = 0.000857$), greenyellow ($r = 0.320$; $p = 0.000529$), light cyan ($r = 0.226$; $p = 0.0156$), grey 60 ($r = 0.196$; $p = 0.0366$), cyan ($r = -0.209$; $p = 0.0257$), magenta ($r = 0.304$; $p = 0.00103$), salmon ($r = -0.308$; $p = 0.000869$), and grey ($r = 0.656$; $p < 0.0001$). Finally, we identified 3 modules that were significantly correlated with color morph, the grey ($r = 0.403$; $p = < 0.0001$), pink ($r = -0.372$; $p = < 0.0001$), and purple modules ($r = 0.190$; $p = 0.042$). Significant GO terms associated with each module that is correlated with species, color morph, and developmental stage are found in Supplemental Tables 7, 8, and 9 respectively.

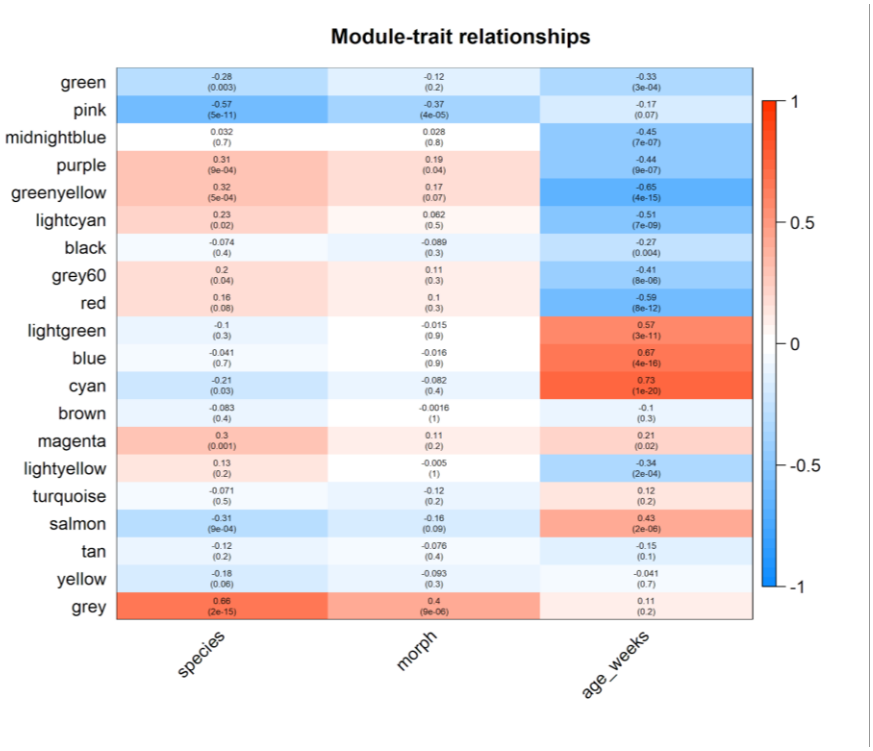

Figure 10. The relationship between WGCNA modules and treatment groups. Within each cell the top number represents the R value (correlation between the grouping and module expression) and the bottom number represents the adjusted p value. The strength of the color (i.e., darker red or darker blue) in the heatmap represents the strength of the association.

Discussion:

The genetic, biochemical, cellular, physiological and morphological mechanisms that control coloration in mimetic systems are of interest because of their substantial impacts on survival. Despite this, these mechanisms are poorly characterized. Further, genetic mechanisms and genomic resources in amphibians are limited and poorly understood, particularly compared to better known groups like mammals and fish. In this study, we examined how gene expression contributes to differential phenotypes within species in a Müllerian mimicry complex of poison

555 frogs. To do this we assembled a high-quality genome for the mimic poison frog *Ranitomeya*
556 *imitator*, which we leveraged to conduct gene expression analyses. Here we describe the resulting
557 *R. imitator* genome assembly and highlight key pathways and genes that likely contribute to
558 differential color production within species, illuminating the mechanisms underlying Müllerian
559 mimicry, and providing a rich foundation upon which future research may be built.
560
561 ***Genome:***
562 Our newly assembled *Ranitomeya imitator* genome is a large, high-quality genome with
563 high genic content. This assembled genome is 6.8 Gbp in length and contains 93% of the expected
564 genes according to our BUSCO results. Further, our genome is relatively contiguous with a contig
565 N50 of over 300 Kbp. For comparison, the *O. pumilio* genome produced with short read
566 technologies had a contig N50 of 385 base pairs and many genic regions were not assembled,
567 presumably because of long intronic regions strewn with repeat elements (Rogers et al. 2018). This
568 dramatic difference in genome contiguity and genic content indicates that long read technologies
569 are, unsurprisingly, critically important and can produce genomes with contiguity spanning large
570 regions, even for species with large genomes containing many long, repetitive regions. Further, the
571 relatively high error rate of current long read technologies does not preclude the ability to
572 assemble and identify genes, as evidenced by our high BUSCO score. This genome is a valuable
573 resource and is well-suited to a variety of future work, especially RNA sequencing analyses like
574 those we present below.
575
576 *Repeat elements in the* Ranitomeya imitator *genome:*

Roughly 50% of our genome assembly was masked as repeats. This is a large proportion of the genome, but not as large as that of the strawberry poison frog (*O. pumilio*), which was estimated to consist of ~70% repeats (Rogers et al. 2018). In comparison, the genome of *Xenopus tropicalis* is a little over one-third repeat elements and *Nanorana parkeri* is ~48% repeats, which are both comparable to a mammalian genome (Hellsten et al. 2010; Sun et al. 2015). Scattered throughout the *R. imitator* genome are a large number of repeat elements which represent over half of the assembled genome. While our assembly of this genome is similar in size to the estimated size of the *Oophaga pumilio* genome, we found a much smaller proportion of particular families of repeat elements (e.g., *Gypsy*) than Rogers et al. (2018) did. Instead, the *R. imitator* genome seems to have a higher evenness of repeat element types spread throughout the genome. A number of the repeat elements that we identified had an average length longer than 1,000 base pairs, including L1 (1,093.4 ± 1,490.5), L1-Tx1 (1,417.3 ± 1,372.3), *Gypsy* (1,349.0 ± 1619.3), and *Pao* (1,254.9 ± 1,385.8). Not only that, but these repeat classes made up a large portion of the genome. Our *R. imitator* genome assembly has less than half the total content for many of the most abundant families of repeats in the strawberry poison frog, including *Gypsy* (0.44 Gbp vs 1 Gbp), *Copia* (3 Mbp vs 298 Mbp), *hAT* (97 Mbp vs 255 Mbp), and *Mariner* (0.6 Mbp vs 197 Mbp). However, *R. imitator* has much more total repeat content of *Tc1* (298 Mbp vs 181 Mbp) and a large portion of the *R. imitator* genome consists of unidentified repeats (25%, 1.87 Gbp). Thus, it seems likely that different families of repeats have proliferated between the two poison frog genomes. However, there are two caveats to this conclusion. First is the proportion of repeats that we were unable to classify in the *R. imitator* genome, and second is that our two studies used very different input data, assembly algorithms, and methods of analyzing repeats (RepDeNovo in *O. pumilio* and RepeatMasker in *R.* imitator) which are a potential source of bias.

Our BUSCO analysis also identified a large number of genes that have been duplicated scattered throughout the genome—23.2% of orthologs expected to be present as a single-copy are in fact present in duplicate copies. These are spread throughout the scaffolds in the genome, and the same repeated ortholog is found at most three times in the genome. The repeats appear almost exclusively in two copies that very rarely appear on the same scaffold. Both copies of a duplicated ortholog only appeared on the same scaffold four times. All of the other duplicated genes were split across scaffolds. Additionally, we found that most single copy orthologs had higher-than-average coverage, whereas most duplicated orthologs had below average coverage. Indeed, relative to single copy orthologs, a larger proportion of duplicated orthologs had particularly low coverage (< 10x).

There are two plausible explanations for this phenomenon. First, this could be driven by historic duplication events (perhaps even chromosomal), followed by sequence divergence and possibly pseudogenization. This would lead to both multiple copies of orthologs as well as mapping ambiguities due to sequence similarities. Alternatively, this evidence, while preliminary, could indicate that some proportion of the large number of duplicated orthologs found in the genome arise from uncollapsed regions of heterozygosity. This is consistent with duplicated orthologs being present in only two copies that often have low coverage.

Gene expression:

While the colors and patterns of *Ranitomeya* poison frogs are extremely variable, they always consist of vivid color patches overlaying a background that is largely black in most color morphs. Recent evidence indicates that much of the differences in color in poison frogs are derived from the structure (thickness) and orientation of iridophore platelets (Twomey, Kain, et al. 2020).

Additionally, specific pigments that are deposited in the xanthophores, such as pteridines and carotenoids, interact with these structural elements to influence integumental coloration (in the yellow to red ranges of hue. Black and brown coloration is produced by melanophores and the melanin pigments found within the chromatophores (Bagnara et al. 1968; Duellman and Trueb 1986)(Duellman and Trueb 1986). These data are corroborated by new genomic data that seem to highlight the importance of pigment production and modification genes such as those in the melanin synthesis pathway (Stuckert et al. 2019; Posso-Terranova and Andrés 2017), pteridine synthesis pathway (Stuckert et al. 2019; Rodríguez et al. 2020) and carotenoid processing pathways (Twomey, Johnson, et al. 2020) for their roles in producing different color morphs in poison frogs.

We conducted a targeted analysis of genes which show convergent expression patterns between the model and mimic. Somewhat surprisingly, there was minimal overlap in genes that were differentially expressed between convergent color morphs in both the model and mimic. Of those genes that were shared, only three were in our a priori color gene list (*edaradd, pkc-3,* and *qdpr*). This seems to indicate one of three things: 1) the pattern of differential gene expression affecting convergent color morph development is largely species-specific, 2) the expression patterns of a small number of genes have a very large effect on color morph divergence, or 3) we have insufficient power to identify these convergent genes. Our slightly less restrictive analysis of genes differentially expressed between any morph in multiple species only yielded an extra 10 color genes, which is again fewer than we would have predicted if convergent phenotypes are being driven by the same mechanisms between species. Overall, these results suggest that the convergent color patterns of these species are likely to have evolved via the expression of distinct underlying genetic and biochemical pathways. These findings are largely corroborated by the gene network analyses (WGNCA), which identified many more gene modules associated with

developmental stage (14) or species (10) than with color morph (3). In sum, color differences are likely to be driven by expression patterns of a few genes of large effect.

As for the genes that were differentially expressed throughout development, many are likely related to body restructuring rather than coloration *per se.* Nevertheless, we identified a number of very promising candidate color genes that are likely to play a role in the production of mimetic phenotypes in this system.

Yellow, orange, and red coloration:

Yellows, oranges, and reds are determined in large part by the presence of pigments deposited within the xanthophores, the outermost layer of chromatophores in the skin (Duellman and Trueb 1986). These pigments are primarily composed of pteridines and carotenoids, and many studies to date have documented that these pigments play a key role in the production of yellows, oranges, and reds (Obika and Bagnara 1964; Grether et al. 2001; Mcgraw, Nolan, and Crino 2006; McLean et al. 2017; Croucher et al. 2013). Given the clear importance of xanthophores, pteridines, and carotenoids in the production of yellows, oranges, and reds, we briefly examine the contribution of genes in all three pathways here, beginning with xanthophore production.

Xanthophores:

We identified a number of key genes that are differentially expressed that are required for the production of xanthophores (Figure 7), notably paired box 7 (*pax7*) and xanthine dehydrogenase (*xdh*). *Pax7* is a transcription factor that is required for establishing and differentiating xanthophores in both embryonic and adult zebrafish (Nord et al. 2016). *Pax7* was differentially expressed between morphs in *R. fantastica,* notably with higher expression in the

orange-banded morph. *Xdh* is sometimes referred to as a xanthophore differentiation marker, as it is found in xanthoblasts and is required for synthesizing the pteridine pigment xanthopterin (Epperlein and Löfberg 1990; Reaume, Knecht, and Chovnick 1991; Parichy et al. 2000). In our study, this gene exhibited differential expression across development in both *R. imitator* and *R. fantastica.* Additionally, we saw differential expression in this gene between *R. imitator* color morphs, with the highest expression in the orange banded morph. Given their roles in xanthophore differentiation, *pax7* and *xdh* are excellent candidates for production of xanthophores across all *Ranitomeya,* and early differences in expression of these genes could lay the groundwork for markedly different colors and patterns.

Pteridine synthesis genes:

Genes and biochemical products in the pteridine pathway are important for pigmentation in the eyes and for vision, as well as for coloration across a wide variety of taxa (e.g., invertebrates, fish, lizards, amphibians), as data from both genetic studies and biochemical assays of pigments point to pteridines as important components of animal coloration. Although a number of genes in the pteridine pathway have been implicated in producing different color patterns, in general the genetic control of pteridine pigmentation is poorly characterized and largely comes from studies of *Drosophila melanogaster (Kim, Kim, and Yim 2013; Braasch, Schartl, and Volff 2007)*. In this study we found a number of key pteridine synthesis genes that were differentially expressed between color morphs (Figure 7). Prominent amongst these are the aforementioned xanthine dehydrogenase (*xdh*), quinoid dihydropteridine reductase (*qdpr*), and 6-pyruvoyltetrahydropterin synthase (*pts*).

692 In addition to its role in early xanthophore lineages, *xdh* appears to be highly conserved and
693 its expression plays a role in the production of pterin-based coloration in a variety of taxa such as
694 spiders (Croucher et al. 2013), fish (Parichy et al. 2000; Salis et al. 2019), and the dendrobatid frogs
695 *D. auratus* and *O. pumilio (Stuckert et al. 2019; Rodríguez et al. 2020)*. Experimental inhibition of
696 *xdh* causes a reduction in the quantity of pterins, resulting in an atypical black appearance in
697 axolotls (Sally K. Frost 1978; S. K. Frost and Bagnara 1979; Thorsteinsdottir and Frost 1986).
698 Additionally, typically green frogs with deficiencies in the *xdh* gene appear blue due to the lack of
699 pterins in the xanthophores (Sally K. Frost 1978; S. K. Frost and Bagnara 1979). As discussed above,
700 *xdh* had the highest expression in the orange banded morph of *R. imitator*. Because *xdh* plays a role
701 in the transformation of pterins into several different yellow pterin pigments such as xanthopterin
702 and isoxanthopterin (Ziegler 2003), differential expression of *xdh* is a plausible mechanism for the
703 production of orange coloration in the banded *R. imitator*. In sum, *xdh* may function in xanthophore
704 production and/or pterin synthesis and is a likely driver of the production of yellow, orange, and
705 green colors in this mimicry system.
706
707 One of the first genes in the pteridine synthesis pathway is 6-pyruvoyltetrahydropterin
708 synthase (*pts*), which is responsible for producing the precursor to both the orange drosopterin
709 pigment as well as yellow sepiapterin pigment. This gene has been implicated in the production of
710 yellow color phenotypes in a variety of systems (McLean et al. 2019; Braasch, Schartl, and Volff
711 2007; Rodríguez et al. 2020), and has been linked to different colors in the poison frog *O. pumilio*
712 *(Rodríguez et al. 2020)*. While the precise mechanism by which this gene affects coloration is
713 unknown, as the above studies indicate, differential expression of *pts* is often found in relation to
714 yellow or orange skin phenotypes. In our study, we identified significant differential expression

715 throughout development in *R. fantastica* and *R. imitator,* with overall expression of this gene
716 increasing throughout development. Additionally, we see differential expression in *pts* between
717 color morphs of *R. variabilis,* with higher expression in the yellow striped morph, particularly close
718 to the end of development. We did not find differential expression of *pts* in *R. imitator.* This
719 indicates that *pts* may be a critical gene in developing yellow pigmentation in *R. variabilis,* but that
720 it may not play the same role in *R. imitator*. Interestingly though, Twomey et al. (Twomey, Johnson,
721 et al. 2020) found that the yellow pterin sepiapterin was only present in very small concentrations
722 in the yellow-striped morph of *R. variabilis.*
723
724 Quinoid dihydropteridine reductase (*qdpr*) is another gene involved in the pteridine
725 synthesis pathway and is known to alter patterns of production of the yellow pigment sepiapterin
726 (Ponzone et al. 2004). We found differential expression in this gene across developmental stages in
727 all three species in this study. Notably, the expression of *qdpr* showed a stark decline over
728 development. *Qdpr* showed a convergent pattern of differential expression between color morphs
729 in both *R. imitator* and *R. fantastica,* in both cases with the highest expression in the redheaded
730 morph, although expression was also high in the yellow striped morph of *R. imitator*. This indicates
731 that qdpr is likely playing a similar role in color production in both the model and mimic species.
732 The *qdpr* gene was also differentially expressed across populations of another species of poison
733 frog, and was only expressed in light blue or green colored morphs which are likely to derive some
734 of the coloration from pteridines (Stuckert et al. 2019). In combination, these studies indicate that
735 *qdpr* may be playing a role in the production of pteridine pigmentation in this system and in
736 amphibians in general, particularly since qdpr alters sepiapterin production (Ponzone et al. 2004).
737

738 *Carotenoid genes:*

739 Carotenoids are important for both yellow and red coloration across a diversity of life forms
740 (McGraw 2006; Toews et al 2017). While carotenoids are clearly an important class of pigments
741 that broadly influence coloration, few known genes contribute to carotenoid based color
742 differences (e.g., *bco2*, *scarb1*, *retsat*), although this is likely an underestimation of the actual
743 number of genes playing a role in carotenoid synthesis and processing given that we are
744 continuously discovering new genes that play these roles (Twomey, Johnson, et al. 2020; Emerling
745 2018). It appears that orange and red colored *Ranitomeya* (outside of *R. imitator)* have slightly
746 higher overall carotenoid concentrations, although these colors are more likely to be derived from
747 the pteridine drosopterin (Twomey et al. 2020). However, different color morphs of *R. imitator*
748 possess similar quantities of carotenoids (Twomey et al. 2020), providing little evidence that
749 carotenoid levels influence coloration in *R. imitator*, but that they may be important in other
750 *Ranitomeya spp*. Intriguingly, Crothers et al (2016) found no relationship between coloration and
751 overall carotenoid abundance in the bright orange Solarte morph of *O. pumilio*, but did find a
752 relationship between total dorsal reflectance and two carotenoids (xanthophyll and a canary
753 xanthophyll ester). Thus, the evidence seems to indicate that overall carotenoid concentrations are
754 not particularly important for red, orange, or yellow colorations, and that instead these colors may
755 be driven by a small subset of carotenoids or pteridines.

756

757 We found differential expression of a number of carotenoid genes across development
758 (e.g., *aldh1a1*, *aldh1a2*, *bco1*, *retsat*, *scarb2*). Although we did not find evidence that many known
759 carotenoid genes are a major contributor to differences between specific color morphs in our
760 study, we did find differential expression of some carotenoid genes between morphs (e.g., *slc2a11,*

761 *ttc39b*). We found that a gene that has recently been putatively linked to carotenoid metabolism,
762 the lipoprotein coding gene tetratricopeptide repeat domain 39B (*ttc39b*), was differentially
763 expressed between color morphs of *R. variabilis* and *R. fantastica* (note the latter finding depends
764 on lowering our stringent alpha value to 0.05; Figure 7). Tetratricopeptide repeat domain 39B is
765 upregulated in orange or red skin in a variety of fish species (Ahi et al. 2020; Salis et al. 2019).
766 Hooper et al (Hooper, Griffith, and Price 2019) found that this gene is associated with bill color in
767 the long-tailed finch, *Poephila acuticauda*, and they hypothesized that *ttc39b* is being used to
768 transport hydrophobic carotenoids to their deposition site. We found that this gene was most
769 highly expressed in the yellow-green spotted morph of *R. variabilis* and the redheaded morph of *R.*
770 *fantastica*, consistent with findings from other gene expression studies. Given the repeat
771 occurrence of this gene in pigmentation studies outlined above, functional validation of *ttc39b* is
772 likely to be informative.
773
774 While we found very few putative carotenoid genes identified in other taxa that were
775 differentially expressed between our color morphs, we nevertheless identified the oxidoreductase
776 activity gene ontology as the primary gene ontology term in the purple module associated with
777 color morphs. In addition to some of the pteridine genes discussed above, this module contains a
778 number of candidates for carotenoid metabolism, including retinol dehydrogenase and a variety of
779 cytochrome p450 genes. A recent study by Twomey et al. (Twomey, Johnson, et al. 2020) identified
780 *CYP3A80* as a novel candidate for carotenoid ketolase that is preferentially expressed in the livers
781 of red *Ranitomeya sirensis.* Our gene ontology analysis results indicate that there may be additional
782 genes strongly influencing carotenoid synthesis and processing in this system that have not been
783 identified in previous studies.

784

785 **Melanophore genes:**

786 Many of the differentially expressed genes in our dataset occurred between developmental
787 stages as tadpoles undergo a complete body reorganization as they prepare to metamorphose. In
788 addition to growth, development, and metamorphosis, during this time tadpoles are producing
789 both the structural chromatophores and the pigments that will be deposited within them. In many
790 species, the distribution of chromatophores that will regulate patterns are set early during
791 development. Of these, melanin-based coloration is the best understood aspect of coloration, in no
792 small part because of a long history of genetic analyses in lab mice (Hoekstra 2006; Hubbard et al.
793 2010). As a result, there are a large number of genes that are known to influence the production of
794 melanin, melanophores, and melanosomes. In vertebrates, black coloration is caused by light
795 absorption by melanin in melanophores (Sköld et al. 2016). Melanophores (and the other
796 chromatophores) originate from populations of cells in the neural crest early in development (Park
797 et al. 2009). The four color morphs of *Ranitomeya* used in this study have pattern elements on top
798 of a generally black dorsum and legs, and therefore melanin-related genes are likely to play a key
799 role in color and pattern, both throughout development and between color morphs.

800

801 Given that a large portion of pigmentation arises during development when we sampled
802 individuals, we found that many of our differentially expressed candidate genes are in this pathway.
803 Prominent amongst these genes are *dct, kit, lef1, mc1r, mitf, mlph, mreg, notch1, notch2, sox9,*
804 *sox10, tyr*, and *tyrp1*, all of which were differentially expressed across development in at least one
805 species. It seems likely these genes are contributing to color production across species given the
806 important roles of each of these genes in melanocyte development and melanin synthesis. In fact,

807 the well-known patterning genes in the notch pathway (e.g., *notch1, notch2*; Figure 8) seem to be
808 important in all three species, as *notch1* was differentially expressed across development in *R.*
809 *imitator* and *R. variabilis,* and *notch2* in *R. fantastica* (Hamada et al. 2014). Expression patterns of
810 melanophore and melanin synthesis genes did not follow a consistent pattern overall and instead
811 were variable. In fact, one of the two a priori color genes that was differentially expressed between
812 convergent morphs in both *R. imitator* and *R. fantastica* showed opposite differential expression
813 patterns. This gene, *pkc-3*, has been implicated in melanocyte proliferation, dendricity, and
814 melanogenesis (Park and Gilchrest 1993), indicating that this gene is likely critically important to the
815 production of brown and black coloration. Different directionality of expression of *pkc-3* between
816 *R. imitator* and *R. fantastica* is a peculiar finding, potentially indicating that this gene is influencing
817 different pathways that are species-specific. Our short read lengths in *R. imitator* preclude
818 adequately testing this hypothesis.
819 We found similar results with *edaradd* (Ectodysplasin-A Receptor-Associated Death
820 Domain), which was differentially expressed between the spotted and striped morphs of *R. imitator*
821 and *R. variabilis*. Like *pkc-3*, while this gene was differentially expressed in both the model and the
822 mimic, it showed different expression patterns between the two species. This gene is known to play
823 a role in ectodermal dysplasia, a catch-all term for a suite of similar human diseases that produce
824 abnormalities of ectodermal structures. Phenotypically these appear as sparse hair, abnormal teeth
825 and hair, and, most relevant to our study, abnormally light pigmentation (Cluzeau et al. 2011).
826 Another gene in this pathway, *edar* (Ectodysplasin A Receptor) was differentially expressed
827 between color morphs of both *R. fantastica* and *R. variabilis*, potentially indicating the importance
828 of the TNFα-related signaling pathway (Reyes-Reali et al. 2018; Cluzeau et al. 2011). The TNFα-
829 related signaling pathway has not been implicated as a driver of color and pattern in any context

outside of ectodermal dysplasia, and thus this indicates a plausible mechanism for coloration in animals that has not yet been identified.

Iridophore genes:

Iridophores are largely responsible for blue (and to a lesser extent green) coloration, which is mainly determined by the reflection of light from iridophores (Bagnara et al. 2007). This depends on the presence and orientation of guanine platelets, where thicker platelets tend to reflect longer wavelengths of light (Ziegler 2003; Bagnara et al. 2007; Saenko et al. 2013). Iridophores are a key component of white, blue, and green coloration. Recently, Twomey et al. (2020) found that variation in coloration in *Ranitomeya* and related poison frogs is largely driven by a combination of the orientation and thickness of the guanine platelets in iridophores. Using a combination of electron microscopy, biochemical pigment analyses, and modeling of the interaction between structural elements in the integument and pigmentation within chromatophores, they found that much more of the variation in coloration (hue) was driven by differences in the guanine platelet thickness of iridophores than expected. We discuss our findings in light of this recent work, with respect to how they can inform future work in conjunction with the results of Twomey et al. (2020).

The precise mechanisms underlying the development of iridophores and the size and orientation of the guanine platelets are unknown. However, previous work has suggested that ADP Ribosylation Factors (ARFs), which are ras-related GTPases that control transport through membranes and organelle structure and Rab GTPases, are likely important in determining the size and orientation of iridophores (Higdon et al. 2013). We found a number of these genes to be differentially expressed between developmental stages (*arf6, dct, dgat2, dock7, dst, edn3, erbb3,*

impdh2, paics, psen1, rab27a, rab27b, rabggta) or color morphs (*anxa1, dock7, dst, erbb3, gart, gne, paics, rab1a, rab27a, rab27b, rab7a, rabggta*) in our study (Figure 9). We also found differential expression of a number of genes that are known to impact guanine or purine synthesis throughout development *(adsl, gart, gas1, fh, qdpr*) and between color morphs (*atic, psat1, qdpr*). A number of these genes *(adsl, dct, dock7, gart, fh, qdpr, psat1, rabggta*) have been implicated in previous work in dendrobatids (Rodríguez et al. 2020; Stuckert et al. 2019) and in other taxa. The genes that have been implicated in previous studies are clearly good candidates for future study. Additionally, the ARFs and Rab GTPases that we identified and that are upregulated in iridophores relative to other chromatophore types in fish (e.g., Higdon et al. 2013) are also good candidates. Unfortunately, our understanding of how these genes affect the development of iridophores is limited, and thus more targeted examinations of iridophore production and pigment production are needed. Notably, a number of epidermis-structuring genes (such as those in the krt family) have been implicated in the production of structural colors (e.g., *krt1, krt2*), although more evidence is needed to verify their role in coloration (Burgon et al. 2020; Stuckert et al. 2019; McGowan et al. 2006; Cui et al. 2016). We identified a number of these that are differentially expressed between color morphs (e.g., *krt1, krt2, krt10, krt14, krt5*). Genes that influence keratin, and organization of the epidermis generally, are good candidates for the production of different colors, as they may produce structural influences on color (via reflectance) in a manner that parallels what we see from guanine platelets. Keratins are known to influence the distribution and arrangement of melanosomes, which impact the ultimate color phenotype of animals (Gu and Coulombe 2007a, [b] 2007). The combination of differential expression between colors and/or color morphs in multiple expression studies and a plausible mechanism for color modification suggest that genes in the

keratin family may well be important for producing color differences, although detailed analyses would need to be conducted to confirm this.

Conclusion:

In this study we examined the molecular mechanisms by which mimetic phenotypes are produced in a Müllerian mimicry system. Through our efforts, we have produced the first high-quality poison frog genome, a 6.8 Gbp, contiguous genome assembly with good genic coverage. We leveraged this to examine gene expression in the skin throughout development of four comimetic morphs from three species of *Ranitomeya.* We identified a large number of genes related to melanophores, melanin production, iridophore production, and guanine synthesis that were differentially expressed throughout development, indicating that many of these are important in the production of pigmentation, albeit not color morph specific coloration. Genes related to xanthophore production, carotenoid pathways, melanin production and melanophore production were rarely differentially expressed between color morphs, however those genes that were differentially expressed may be critically important in producing polytypic differences within species that drive mimetic phenotypes. Our results indicate that divergence between color morphs seems to be mainly the result of differences in expression and/or timing of expression, but that convergence for the same color pattern may not be obtained through the same changes in gene expression between species. We identified the importance of the pteridine synthesis pathway in producing these different yellow, orange, and red color morphs across species. Thus, production of these colors are likely strongly driven by differences in gene expression in genes in the pteridine synthesis pathway, and our data indicate that there may be species-specific differences in this

pathway used in producing similar colors and patterns. Further, we highlight the potential importance of genes in the keratin family for producing differential color via structural mechanisms.

Funding:

Funding for this project was provided by an East Carolina University Thomas Harriot College of Arts and Sciences Advancement Council Distinguished Professorship and NSF DEB 165536 to KS, NSF DEB 1655585 to MDM, XSEDE XRAC MCB110134 to MDM and AMMS andMC received support from Agence Nationale de la Recherche (ANR) grants RANAPOSA (ref. ANR-20-CE02-0003), from an "Investissement d'Avenir" grant CEBA (ref. ANR-10-LABX-25-01) and from a Marie Sklodowska-Curie fellowship (FITINV, N 655857).

Acknowledgements:

We are grateful to many individuals for their help with frog husbandry in the lab, including but not limited to M Yoshioka, C Meeks, A Sorokin, K Weinfurther, R Sen, N Davison, M Johnson, M Pahl, N Aramburu, M Tuatama, R Mori-Pezo, J Richard and S Gallusser. We are also grateful to Laura Bauza-Davila for her work doing RNA extractions, and Andrew Lang for guidance converting RNA to cDNA and preparing samples for sequencing. We are grateful to the anonymous reviewers and editors whose comments improved this manuscript.

Author contributions:

Designed research: AMMS, MC, MM, RN, KS, MDM

Performed research: AMMS, MC, MM, KS, TL

Analyzed data: AMMS, TLP

Contributed to writing: AMMS, MC, MM, TLP, TL, RN, KS, MDM

References:

Ahi, Ehsan Pashay, Laurène A. Lecaudey, Angelika Ziegelbecker, Oliver Steiner, Ronald Glabonjat, Walter Goessler, Victoria Hois, Carina Wagner, Achim Lass, and Kristina M. Sefc. 2020. "Comparative Transcriptomics Reveals Candidate Carotenoid Color Genes in an East African Cichlid Fish." *BMC Genomics* 21 (1): 54.

Anders, Simon, Paul Theodor Pyl, and Wolfgang Huber. 2015. "HTSeq—a Python Framework to Work with High-Throughput Sequencing Data." *Bioinformatics* 31 (2): 166–69.

Bankevich, Anton, Sergey Nurk, Dmitry Antipov, Alexey A. Gurevich, Mikhail Dvorkin, Alexander S. Kulikov, Valery M. Lesin, et al. 2012. "SPAdes: A New Genome Assembly Algorithm and Its Applications to Single-Cell Sequencing." *Journal of Computational Biology: A Journal of Computational Molecular Cell Biology* 19 (5): 455–77.

Bao, Weidong, Kenji K. Kojima, and Oleksiy Kohany. 2015. "Repbase Update, a Database of Repetitive Elements in Eukaryotic Genomes." *Mobile DNA* 6 (June): 11.

Beddard, Frank Evers. 1892. *Animal Coloration: An Account of the Principal Facts and Theories Relating to the Colours and Markings of Animals*. S. Sonnenschein & Company.

Benjamini, Yoav, and Yosef Hochberg. 1995. "Controlling the False Discovery Rate: A Practical and Powerful Approach to Multiple Testing." *Journal of the Royal Statistical Society: Series B (Methodological)*. https://doi.org/10.1111/j.2517-6161.1995.tb02031.x.

Bolger, Anthony M., Marc Lohse, and Bjoern Usadel. 2014. "Trimmomatic: A Flexible Trimmer for Illumina Sequence Data." *Bioinformatics* 30 (15): 2114–20.

Braasch, Ingo, Manfred Schartl, and Jean Nicolas Volff. 2007. "Evolution of Pigment Synthesis Pathways by Gene and Genome Duplication in Fish." *BMC Evolutionary Biology* 7: 1–18.

Briolat, Emmanuelle S., Emily R. Burdfield-Steel, Sarah C. Paul, Katja H. Rönkä, Brett M. Seymoure, Theodore Stankowich, and Adam M. M. Stuckert. 2019. "Diversity in Warning Coloration: Selective Paradox or the Norm?" *Biological Reviews of the Cambridge Philosophical Society* 94 (2): 388–414.

Brown, Jason L., Evan Twomey, Adolfo Amezquita, Moises B. DeSouza, Janalee Caldwell, Stefan Lötters, Rudolf Von May, et al. 2011. "A Taxonomic Revision of the Neotropical Poison Frog Genus *Ranitomeya* (Amphibia: Dendrobatidae)." *Zootaxa* 3083: 1–120.

Burgon, James D., David R. Vieites, Arne Jacobs, Stefan K. Weidt, Helen M. Gunter, Sebastian Steinfartz, Karl Burgess, Barbara K. Mable, and Kathryn R. Elmer. 2020. "Functional Colour Genes and Signals of Selection in Colour-polymorphic Salamanders." *Molecular Ecology* 29 (7): 1284–99.

Campbell, Michael S., Carson Holt, Barry Moore, and Mark Yandell. 2014. "Genome Annotation and Curation Using MAKER and MAKER-P." *Current Protocols in Bioinformatics / Editoral Board, Andreas D. Baxevanis ... [et Al.]* 48 (1): 188.

Coombe, Lauren, Jessica Zhang, Benjamin P. Vandervalk, Justin Chu, Shaun D. Jackman, Inanc Birol, and René L. Warren. 2018. "ARKS: Chromosome-Scale Scaffolding of Human Genome Drafts with Linked Read Kmers." *BMC Bioinformatics* 19 (1): 234.

Croucher, Peter J. P., Michael S. Brewer, Christopher J. Winchell, Geoff S. Oxford, and Rosemary G. Gillespie. 2013. "De Novo Characterization of the Gene-Rich Transcriptomes of Two Color-Polymorphic Spiders, Theridion Grallator and T. Californicum (Araneae: Theridiidae), with Special Reference to Pigment Genes." *BMC Genomics* 14 (1): 862.

Cui, Yucong, Yajun Song, Qingling Geng, Zengfeng Ding, Yilong Qin, Ruiwen Fan, Changsheng Dong, and Jianjun Geng. 2016. "The Expression of KRT2 and Its Effect on Melanogenesis in Alpaca

968 Skins." *Acta Histochemica* 118 (5): 505–12.
969 Dobin, Alexander, Carrie A. Davis, Felix Schlesinger, Jorg Drenkow, Chris Zaleski, Sonali Jha, Philippe
970 Batut, Mark Chaisson, and Thomas R. Gingeras. 2013. "STAR: Ultrafast Universal RNA-Seq
971 Aligner." *Bioinformatics* 29 (1): 15–21.
972 Duellman, William E., and Linda Trueb. 1986. *Biology of Amphibians*. Baltimore: The John Hopkins
973 University Press.
974 DuShane, Graham P. 1935. "An Experimental Study of the Origin of Pigment Cells in Amphibia." *The*
975 *Journal of Experimental Zoology* 72 (1): 1–31.
976 Eden, Eran, Roy Navon, Israel Steinfeld, Doron Lipson, and Zohar Yakhini. 2009. "GOrilla: A Tool for
977 Discovery and Visualization of Enriched GO Terms in Ranked Gene Lists." *BMC Bioinformatics*
978 10 (February): 48.
979 Emerling, Christopher A. 2018. "Independent Pseudogenization of CYP2J19 in Penguins, Owls and
980 Kiwis Implicates Gene in Red Carotenoid Synthesis." *Molecular Phylogenetics and Evolution*
981 118 (January): 47–53.
982 Epperlein, H. H., and J. Löfberg. 1990. "The Development of the Larval Pigment Patterns in Triturus
983 Alpestris and Ambystoma Mexicanum." *Advances in Anatomy, Embryology, and Cell Biology*
984 118: 1–99.
985 Fox, Denis L. 1936. "Structural and Chemical Aspects of Animal Coloration." *The American*
986 *Naturalist* 70 (730): 477–93.
987 Frost, Sally K. 1978. "Developmental Aspects of Pigmentation in the Mexican Leaf Frog,
988 *Pachymedusa Dacnicolor*."
989 Frost, S. K., and J. T. Bagnara. 1979. "Allopurinol-Induced Melanism In The Tiger Salamander
990 (Ambystoma Iigrinum Nebulosum)." *The Journal of Experimental Zoology* 209 (3): 455–65.
991 Funk, W. Chris, Kelly R. Zamudio, and Andrew J. Crawford. 2018. "Advancing Understanding of
992 Amphibian Evolution, Ecology, Behavior, and Conservation with Massively Parallel
993 Sequencing." *Population Genomics*. https://doi.org/10.1007/13836_2018_61.
994 Grabherr, Manfred G., Brian J. Haas, Moran Yassour, Joshua Z. Levin, Dawn A. Thompson, Ido Amit,
995 Xian Adiconis, et al. 2011. "Full-Length Transcriptome Assembly from RNA-Seq Data without a
996 Reference Genome." *Nature Biotechnology* 29 (7): 644–52.
997 Gray, Suzanne M., and Jeffrey S. McKinnon. 2007. "Linking Color Polymorphism Maintenance and
998 Speciation." *Trends in Ecology & Evolution* 22 (2): 71–79.
999 Grether, Gregory F., David F. Millie, Michael J. Bryant, David N. Reznick, and Wendy Mayea. 2001.
1000 "RAIN FOREST CANOPY COVER, RESOURCE AVAILABILITY, AND LIFE HISTORY EVOLUTION IN
1001 GUPPIES." *Ecology* 82 (6): 1546–59.
1002 Gu, Li-Hong, and Pierre A. Coulombe. 2007a. "Keratin Function in Skin Epithelia: A Broadening
1003 Palette with Surprising Shades." *Current Opinion in Cell Biology* 19 (1): 13–23.
1004 ———. 2007b. "Keratin Expression Provides Novel Insight into the Morphogenesis and Function of
1005 the Companion Layer in Hair Follicles." *The Journal of Investigative Dermatology* 127 (5):
1006 1061–73.
1007 Hamada, Hiroki, Masakatsu Watanabe, Hiu Eunice Lau, Tomoki Nishida, Toshiaki Hasegawa, David
1008 M. Parichy, and Shigeru Kondo. 2014. "Involvement of Delta/Notch Signaling in Zebrafish Adult
1009 Pigment Stripe Patterning." *Development* 141 (2): 318–24.
1010 Hellsten, Uffe, Richard M. Harland, Michael J. Gilchrist, David Hendrix, Jerzy Jurka, Vladimir
1011 Kapitonov, Ivan Ovcharenko et al. "The genome of the Western clawed frog Xenopus
1012 tropicalis." *Science* 328, no. 5978 (2010): 633-636.
1013 Hodges, Scott A., and Nathan J. Derieg. 2009. "Adaptive Radiations: From Field to Genomic

1014 Studies." *Proceedings of the National Academy of Sciences of the United States of America* 106
1015 Suppl 1 (June): 9947–54.
1016 Hoekstra, H. E. 2006. "Genetics, Development and Evolution of Adaptive Pigmentation in
1017 Vertebrates." *Heredity* 97 (3): 222–34.
1018 Hooper, Daniel M., Simon C. Griffith, and Trevor D. Price. 2019. "Sex Chromosome Inversions
1019 Enforce Reproductive Isolation across an Avian Hybrid Zone." *Molecular Ecology* 28 (6): 1246–
1020 62.
1021 Hubbard, Joanna K., J. Albert C. Uy, Mark E. Hauber, Hopi E. Hoekstra, and Rebecca J. Safran. 2010.
1022 "Vertebrate Pigmentation: From Underlying Genes to Adaptive Function." *Trends in Genetics:*
1023 *TIG* 26 (5): 231–39.
1024 Kang, Changku, Thomas N. Sherratt, Ye Eun Kim, Yujin Shin, Jongyeol Moon, Uhram Song, Jae Yeon
1025 Kang, Kyungmin Kim, and Yikweon Jang. 2017. "Differential Predation Drives the Geographical
1026 Divergence in Multiple Traits in Aposematic Frogs." *Behavioral Ecology: Official Journal of the*
1027 *International Society for Behavioral Ecology* 00: 1–9.
1028 Kim, Heuijong, Kiyoung Kim, and Jeongbin Yim. 2013. "Biosynthesis of Drosopterins, the Red Eye
1029 Pigments of Drosophila Melanogaster." *IUBMB Life* 65 (4): 334–40.
1030 Kronforst, Marcus R., and Riccardo Papa. 2015. "The Functional Basis of Wing Patterning in
1031 *Heliconius* Butterflies: The Molecules behind Mimicry." *Genetics* 200 (1): 1–19.
1032 Langfelder, Peter, and Steve Horvath. 2008. "WGCNA: An R Package for Weighted Correlation
1033 Network Analysis." *BMC Bioinformatics* 9 (December): 559.
1034 Li, H., and R. Durbin. 2009. "Fast and Accurate Short Read Alignment with Burrows–Wheeler
1035 Transform." *Bioinformatics* . https://academic.oup.com/bioinformatics/article-
1036 abstract/25/14/1754/225615.
1037 Li, Heng. 2018. "Minimap2: Pairwise Alignment for Nucleotide Sequences." *Bioinformatics* 34 (18):
1038 3094–3100.
1039 Li, Heng, Bob Handsaker, Alec Wysoker, Tim Fennell, Jue Ruan, Nils Homer, Gabor Marth, Goncalo
1040 Abecasis, Richard Durbin, and 1000 Genome Project Data Processing Subgroup. 2009. "The
1041 Sequence Alignment/Map Format and SAMtools." *Bioinformatics* 25 (16): 2078–79.
1042 Longley, W. H. 1917. "Studies Upon the Biological Significance of Animal Coloration. II. A Revised
1043 Working Hypothesis of Mimicry." *The American Naturalist* 51 (605): 257–85.
1044 Love, Michael, Simon Anders, and Wolfgang Huber. 2014. "Differential Analysis of Count Data--the
1045 DESeq2 Package." *Genome Biology* 15 (550): 10–1186.
1046 MacManes, Matthew D. 2018. "The Oyster River Protocol: A Multi-Assembler and Kmer Approach
1047 for de Novo Transcriptome Assembly." *PeerJ* 6: e5428.
1048 Mallet, James, and Nicholas H. Barton. 1989. "Strong Natural Selection in a Warning-Color Hybrid
1049 Zone." *Evolution; International Journal of Organic Evolution* 43 (2): 421–31.
1050 Marek, Paul E., and Jason E. Bond. 2009. "A Müllerian Mimicry Ring in Appalachian Millipedes."
1051 *Proceedings of the National Academy of Sciences of the United States of America* 106 (24):
1052 9755–60.
1053 Marks, Patrick, Sarah Garcia, Alvaro Martinez Barrio, Kamila Belhocine, Jorge Bernate, Rajiv
1054 Bharadwaj, Keith Bjornson, et al. 2019. "Resolving the Full Spectrum of Human Genome
1055 Variation Using Linked-Reads." *Genome Research* 29 (4): 635–45.
1056 Martin, A., R. Papa, N. J. Nadeau, R. I. Hill, B. A. Counterman, G. Halder, C. D. Jiggins, et al. 2012.
1057 "Diversification of Complex Butterfly Wing Patterns by Repeated Regulatory Evolution of a
1058 Wnt Ligand." *Proceedings of the National Academy of Sciences* 109 (31): 12632–37.
1059 McGowan, Kelly A., Swaroop Aradhya, Helmut Fuchs, Martin H. de Angelis, and Gregory S. Barsh.

2006. “A Mouse Keratin 1 Mutation Causes Dark Skin and Epidermolytic Hyperkeratosis.” *The Journal of Investigative Dermatology* 126 (5): 1013–16.
Mcgraw, K. J., P. M. Nolan, and O. L. Crino. 2006. “Carotenoid Accumulation Strategies for Becoming a Colourful House Finch: Analyses of Plasma and Liver Pigments in Wild Moulting Birds.” *Functional Ecology* 20 (4): 678–88.
McLean, Claire A., Adrian Lutz, Katrina J. Rankin, Adam Elliott, Adnan Moussalli, and Devi Stuart-Fox. 2019. “Red Carotenoids and Associated Gene Expression Explain Colour Variation in Frillneck Lizards.” *Proceedings. Biological Sciences / The Royal Society* 286 (1907): 20191172.
McLean, Claire A., Adrian Lutz, Katrina J. Rankin, Devi Stuart-Fox, and Adnan Moussalli. 2017. “Revealing the Biochemical and Genetic Basis of Color Variation in a Polymorphic Lizard.” *Molecular Biology and Evolution* 34 (8): 1924–35.
Nord, Hanna, Nils Dennhag, Joscha Muck, and Jonas von Hofsten. 2016. “Pax7 Is Required for Establishment of the Xanthophore Lineage in Zebrafish Embryos.” *Molecular Biology of the Cell* 27 (11): 1853–62.
Obika, M., and J. T. Bagnara. 1964. “PTERIDINES AS PIGMENTS IN AMPHIBIANS.” *Science* 143 (3605): 485–87.
Parichy, D. M., D. G. Ransom, B. Paw, L. I. Zon, and S. L. Johnson. 2000. “An Orthologue of the Kit-Related Gene Fms Is Required for Development of Neural Crest-Derived Xanthophores and a Subpopulation of Adult Melanocytes in the Zebrafish, Danio Rerio.” *Development* 127 (14): 3031–44.
Park, H. Y., M. Kosmadaki, M. Yaar, and B. A. Gilchrest. 2009. “Cellular Mechanisms Regulating Human Melanogenesis.” *Cellular and Molecular Life Sciences: CMLS* 66 (9): 1493–1506.
Ponzone, Alberto, Marco Spada, Silvio Ferraris, Irma Dianzani, and Luisa De Sanctis. 2004. “Dihydropteridine Reductase Deficiency in Man: From Biology to Treatment.” *Medicinal Research Reviews* 24 (2): 127–50.
Posso-Terranova, Andrés, and José Á. Andrés. 2017. “Diversification and Convergence of Aposematic Phenotypes: Truncated Receptors and Cellular Arrangements Mediate Rapid Evolution of Coloration in Harlequin Poison Frogs.” *Evolution; International Journal of Organic Evolution* 71 (11): 2677–92.
Reaume, A. G., D. A. Knecht, and A. Chovnick. 1991. “The Rosy Locus in Drosophila Melanogaster: Xanthine Dehydrogenase and Eye Pigments.” *Genetics* 129 (4): 1099–1109.
Reed, Robert D., Riccardo Papa, Arnaud Martin, Heather M. Hines, Marcus R. Kronforst, Rui Chen, Georg Halder, H. Frederik Nijhout, and W. Owen Mcmillan. 2011. “Optix Drives the Repeated Convergent Evolution of Butterfly Wing Pattern Mimicry.” *Science* 333 (August): 1137–41.
Robertson, Gordon, Jacqueline Schein, Readman Chiu, Richard Corbett, Matthew Field, Shaun D. Jackman, Karen Mungall, et al. 2010. “De Novo Assembly and Analysis of RNA-Seq Data.” *Nature Methods* 7 (11): 909–12.
Rodríguez, Ariel, Nicholas I. Mundy, Roberto Ibáñez, and Heike Pröhl. 2020. “Being Red, Blue and Green: The Genetic Basis of Coloration Differences in the Strawberry Poison Frog (Oophaga Pumilio).” *BMC Genomics* 21 (1): 301.
Rogers, Rebekah L., Long Zhou, Chong Chu, Roberto Márquez, Ammon Corl, Tyler Linderoth, Layla Freeborn, et al. 2018. “Genomic Takeover by Transposable Elements in the Strawberry Poison Frog.” *Molecular Biology and Evolution* 35 (12): 2913–27.
Ruan, Jue, and Heng Li. 2019. “Fast and Accurate Long-Read Assembly with wtdbg2.” *Nature Methods*, December. https://doi.org/10.1038/s41592-019-0669-3.
Rudh, Andreas, and Anna Qvarnström. 2013. “Adaptive Colouration in Amphibians.” *Seminars in*

Cell & Developmental Biology 24 (6-7): 553–61.
Ruxton, G. D., T. N. Sherratt, and M. P. Speed. 2004. *Avoiding Attack: The Evolutionary Ecology of Crypsis, Warning Signals and Mimicry*. Vol. 17.
Salis, Pauline, Thibault Lorin, Victor Lewis, Carine Rey, Anna Marcionetti, Marie-Line Escande, Natacha Roux, et al. 2019. "Developmental and Comparative Transcriptomic Identification of Iridophore Contribution to White barring in Clownfish." *Pigment Cell & Melanoma Research* 32 (3): 391–402.
Schulte, Rainer. 1986. "Eine Neue Dendrobates—art Aus Ostperu (Amphibia: Salienta: Dendrobatidae)." *Sauria* 8: 11–20.
Sherratt, Thomas N. 2006. "Spatial Mosaic Formation through Frequency-Dependent Selection in M??llerian Mimicry Complexes." *Journal of Theoretical Biology* 240 (2): 165–74.
———. 2008. "The Evolution of Müllerian Mimicry." *Die Naturwissenschaften* 95 (8): 681–95.
Simão, Felipe A., Robert M. Waterhouse, Panagiotis Ioannidis, Evgenia V. Kriventseva, and Evgeny M. Zdobnov. 2015. "BUSCO: Assessing Genome Assembly and Annotation Completeness with Single-Copy Orthologs." *Bioinformatics* 31 (19): 3210–12.
Sköld, Helen Nilsson, Sara Aspengren, Karen L. Cheney, and Margareta Wallin. 2016. "Fish Chromatophores-From Molecular Motors to Animal Behavior." *International Review of Cell and Molecular Biology* 321: 171–219.
Smit, A. F. A., and R. Hubley. 2008-2015. *RepeatModeler Open-1.0*. http://www.repeatmasker.org.
Smit, A. F. A., R. Hubley, and P. Green. 2013-2015. *RepeatMasker Open-4.0*. http://www.repeatmasker.org.
Stuckert, Adam M. M., Emily Moore, Kaitlin P. Coyle, Ian Davison, Matthew D. MacManes, Reade Roberts, and Kyle Summers. 2019. "Variation in Pigmentation Gene Expression Is Associated with Distinct Aposematic Color Morphs in the Poison Frog, Dendrobates Auratus." *BMC Evolutionary Biology* 19 (85): 1–15.
Stuckert, Adam M. M., Ralph A. Saporito, Pablo J. Venegas, and Kyle Summers. 2014. "Alkaloid Defenses of Co-Mimics in a Putative Müllerian Mimetic Radiation." *BMC Evolutionary Biology* 14: 1–8.
Stuckert, Adam M. M., Pablo J. Venegas, and Kyle Summers. 2014. "Experimental Evidence for Predator Learning and Müllerian Mimicry in Peruvian Poison Frogs (Ranitomeya, Dendrobatidae)." *Evolutionary Ecology* 28 (3): 413–26.
Stuckert, Adam M. M. and Troy M. LaPolice. (2021). "AdamStuckert/Ranitomeya_imitator_genome: The genomics of mimicry: gene expression throughout development provides insights into convergent and divergent phenotypes in a Müllerian mimicry system (Version v1.0)." *Zenodo*. http://doi.org/10.5281/zenodo.4758404.
Stuckert, Adam M. M. Mathieu Chouteau, Melanie McClure, Troy M LaPolice, Tyler Linderoth, Rasmus Nielsen, … Matthew D MacManes. (2021). "The genomics of mimicry: gene expression throughout development provides insights into convergent and divergent phenotypes in a Müllerian mimicry system." *Zenodo*. http://doi.org/10.5281/zenodo.4758346.
Sun, Yan-Bo, Zi-Jun Xiong, Xue-Yan Xiang, Shi-Ping Liu, Wei-Wei Zhou, Xiao-Long Tu, Li Zhong et al. "Whole-genome sequence of the Tibetan frog *Nanorana parkeri* and the comparative evolution of tetrapod genomes." Proceedings of the National Academy of Sciences 112, no. 11 (2015): E1257-E1262.
Supple, Megan a., Heather M. Hines, Kanchon K. Dasmahapatra, James J. Lewis, Dahlia M. Nielsen, Christine Lavoie, David a. Ray, Camilo Salazar, W. Owen Mcmillan, and Brian a. Counterman. 2013. "Genomic Architecture of Adaptive Color Pattern Divergence and Convergence in

Heliconius Butterflies." *Genome Research* 23 (662): 1248–57.
Symula, R., R. Schulte, and K. Summers. 2001. "Molecular Phylogenetic Evidence for a Mimetic Radiation in Peruvian Poison Frogs Supports a Müllerian Mimicry Hypothesis." *Proceedings of the Royal Society B: Biological Sciences* 268 (1484): 2415–21.
———. 2003. "Molecular Systematics and Phylogeography of Amazonian Poison Frogs of the Genus *Dendrobates*." *Molecular Phylogenetics and Evolution* 26 (3): 452–75.
Team, R. Core. 2019. "R: A Language and Environment for Statistical computing(Version 3.6. 0)[Computer Software]. R Foundation for Statistical Computing, Vienna, Austria."
Thorsteinsdottir, Solveig, and Sally K. Frost. 1986. "Pigment Cell Differentiation: The Relationship between Pterin Content, Allopurinol Treatment, and the Melanoid Gene in Axolotls." *Cell Differentiation* 19: 161–72.
Twomey, Evan, James D. Johnson, Santiago Castroviejo-Fisher, and Ines Van Bocxlaer. 2020. "A Ketocarotenoid-Based Color Polymorphism in the Sira Poison Frog Ranitomeya Sirensis Indicates Novel Gene Interactions Underlying Aposematic Signal Variation." *Molecular Ecology*. https://onlinelibrary.wiley.com/doi/abs/10.1111/mec.15466?casa_token=HfW3FcMDWEsAAAAA:4WvPeH_f3rgYyvO-PmCh18EPVKnr3kW3KSxksgWbdPYhWPyJk20QEbdD3osOTofr6V-F43rVbVH9fA.
Twomey, Evan, Morgan Kain, Myriam Claeys, Kyle Summers, Santiago Castroviejo-Fisher, and Ines Van Bocxlaer. 2020. "Mechanisms for Color Convergence in a Mimetic Radiation of Poison Frogs." *The American Naturalist*, January. https://doi.org/10.1086/708157.
Twomey, Evan, Justin Yeager, Jason Lee Brown, Victor Morales, Molly Cummings, and Kyle Summers. 2013. "Phenotypic and Genetic Divergence among Poison Frog Populations in a Mimetic Radiation." Edited by Pawel Michalak. *PloS One* 8 (2): e55443.
Walker, Bruce J., Thomas Abeel, Terrance Shea, Margaret Priest, Amr Abouelliel, Sharadha Sakthikumar, Christina A. Cuomo, et al. 2014. "Pilon: An Integrated Tool for Comprehensive Microbial Variant Detection and Genome Assembly Improvement." *PloS One* 9 (11): e112963.
Warren, Rene L. 2016. "RAILS and Cobbler: Scaffolding and Automated Finishing of Draft Genomes Using Long DNA Sequences." *J. Open Source Software* 1 (7): 116.
Weisenfeld, Neil I., Vijay Kumar, Preyas Shah, Deanna M. Church, and David B. Jaffe. 2017. "Direct Determination of Diploid Genome Sequences." *Genome Research* 27 (5): 757–67.
Wickham, Hadley. 2011. "ggplot2." *Wiley Interdisciplinary Reviews: Computational Statistics* 3 (2): 180–85.
Wilson, Joseph S., Joshua P. Jahner, Matthew L. Forister, Erica S. Sheehan, Kevin A. Williams, and James P. Pitts. 2015. "North American Velvet Ants Form One of the World's Largest Known Müllerian Mimicry Complexes." *Current Biology: CB* 25 (16): R704–6.
Xu, Gui-Cai, Tian-Jun Xu, Rui Zhu, Yan Zhang, Shang-Qi Li, Hong-Wei Wang, and Jiong-Tang Li. 2019. "LR_Gapcloser: A Tiling Path-Based Gap Closer That Uses Long Reads to Complete Genome Assembly." *GigaScience* 8 (1). https://doi.org/10.1093/gigascience/giy157.
Ziegler, Irmgard. 2003. "The Pteridine Pathway in Zebrafish: Regulation and Specification during the Determination of Neural Crest Cell-Fate." *Pigment Cell Research / Sponsored by the European Society for Pigment Cell Research and the International Pigment Cell Society* 16 (3): 172–82.

Supplemental Materials

SUPPLEMENTAL METHODS:

Genome assembly:

Annotations using Maker:

We annotated our genome using Maker version 3.01.02 (Campbell et al. 2014). We used transcript evidence from *Ranitomeya imitator* to aid in assembly ("est2genome=1"). These data include: 1) a developmental series of tadpole skin across color morphs of captive bred *R. imitator* (this paper, see below), 2) liver, skin, and intestine samples from six different wild *R. imitator* populations (Stuckert et al. unpublished data), and 3) brain samples from captive bred *R. imitator* (Geralds et al. unpublished data). The developmental series data were used in order to accurately annotate genes that are expressed in the skin at different time points in order to target color genes. The addition of data from wild frogs and a variety of other tissue types were used to provide additional transcript evidence in an effort to recover more genes after annotation.

Transcriptome assemblies:

Developmental series:

We used data from the imitator developmental series we analyzed in this paper to make transcriptome across developmental time points in the skin. In order to generate an initial reference transcriptome we assembled 40 M randomly subsampled forward and reverse reads sampled across morphs and time points using seqtk (https://github.com/lh3/seqtk) and used the Oyster River Protocol version 1.1.1 (MacManes 2017) to assemble this dataset. Evidence indicates that there is a substantial diminishment of returns in terms of transcriptome assembly completeness from using over 20-30 million reads (MacManes 2017). Initial error correction was done using RCorrector 1.01, followed by adaptor removal and quality trimming using trimmomatic version 0.36 at a Phred score of ≤ 3 (Bolger et al. 2014) since overly aggressive quality trimming has been shown to reduce assembly completeness (MacManes 2014). The Oyster River Protocol (MacManes 2017) assembles a transcriptome by merging multiple assemblies constructed using a series of different transcriptome assemblers and kmer lengths. We constructed the Independent assemblies with Trinity version 2.4.0 (Grabherr et al. 2011), Shannon version 0.0.2 (Kannan et al. 2016), and SPAdes assembler version 3.11 using 35-mers (Bankevich et al. 2012). This deviates slightly from the Oyster River Protocol specified in MacManes (2017), which specifies kmer lengths of 55 and 75 for SPAdes assemblies, but that exceeds our 50 bp sequencing read length. We then merged these individual assemblies using OrthoFuser (MacManes 2017). Finally, we assessed transcriptome quality using BUSCO version 3.0.1 (Simão et al. 2015) and TransRate 1.0.3 (Smith-Unna et al. 2016).

Transcriptomes from wild frogs of multiple populations:

We *de novo* assembled transcriptomes from six populations along a transition zone from the orange banded morph of *R. imitator* (*R. summersi* mimic) through the yellow striped morph (lowland *R. variabilis* mimic). This includes two pure orange banded populations, two pure yellow striped populations, and two admixed populations with highly variable phenotypes. For each population we randomly chose one individual, concatenated Illumina HiSeq 4000 reads from the liver, intestines, and dorsal skin into a single readset per population and then used the Oyster River Protocol version 2.2.8 (MacManes 2018) to assemble population specific *de novo* transcriptomes. This is similar to the approach above in the section "*Developmental series*", with some minor differences which we detail here. First, we assembled individual assemblies using Trinity version

2.8.5 (Grabherr et al. 2011), two iterations of SPAdes version 3.13.1 (Bankevich et al. 2012) with kmer values of 55 and 75 respectively, and finally Trans-ABySS version 2.0.1 (Robertson et al. 2010). These individually built transcriptomes were then merged together using OrthoFuser (MacManes 2018). Unique contigs which were dropped in Orthofuser were recovered using a reciprocal blast search of the final assembly against the individual assemblies for unique contigs. We removed all contigs with expression lower than one Transcript Per Million (TPM) using the TPM=1 flag in the ORP. Contigs that were dropped due to low expression but which likely represent expressed genes were recovered by blasting these against the UniProt database. Finally, transcriptome quality was assessed using BUSCO version 3.0.1 (Simão et al. 2015) and TransRate 1.0.3 (Smith-Unna et al. 2016).

Brain transcriptome assemblies:

Geralds et al. (unpublished data) conducted an experiment looking at the effects of parental behaviors and tadpole begging on gene expression in the brains of adult *Ranitomeya imitator*. We randomly chose one individual from individuals that were interacting with begging tadpoles, and those that were not. We concatenated these data into a single forward and reverse read file, then used the Oyster River Protocol version 2.2.8 (MacManes 2018) to assemble the brain transcriptome. These details are the same as above in the "*Transcriptomes from wild frogs of multiple populations"* section.

Gene expression:

Ranitomeya imitator:

Frogs from our study populations were collected by Understory and captive bred in Peru prior to shipping captive-bred frogs to a breeding facility in Canada. We purchased individuals that were captive bred in Canada. The frogs used in this study have a similar phenotype to those of individuals found in captivity from their source populations. As with any captive stock sourced from the wild, there is likely an initial bottleneck and corollary reduction in overall heterozygosity, however morphs were not selectively bred to produce desired phenotypes.

Breeding *R. imitator* pairs were placed in 5-gallon terraria containing small (approximately 13 cm) PVC pipes capped on one end and filled halfway with water. We removed tadpoles from the tanks after the male transported them into the pools of water and hand reared them. Although in the wild female *R. imitator* feed their tadpoles unfertilized eggs, tadpoles can survive and thrive on other food items (Brown et al. 2008). We raised experimental tadpoles on a diet of Omega One Marine Flakes fish food mixed with Freeze Dried Argent Cyclop-Eeze, which they received three times a week, with full water changes twice a week until sacrificed for analyses at 2, 4, 7, and 8 weeks of age. At two weeks, tadpoles are limbless, patternless, and a light gray color with two dark black eyeballs. At 4 weeks tadpoles are a slightly darker gray and have back limb buds. Tadpoles had developed their pattern and some coloration as well as reached the onset of metamorphosis at around week 7, and had metamorphosed, were resorbing the tail, and had their froglet patterns at 8 weeks old. Pattern development continues as juveniles and subadults frogs as they grow into the ultimate pattern they possess as adults. Our four sampling periods correspond to roughly Gosner stages 25, 27, 42, and 44 (Gosner 1960). Tadpoles were raised in a homogenous environment, and thus tadpoles were generally at the same developmental stage at the point of sacrifice. Due to inherent variation, some individuals may have been one Gosner stage off the norm. We sequenced a minimum of three individuals at each time point from the Sauce, Tarapoto, and Varadero

populations (except for Tarapoto at 8 weeks), and two individuals per time point from the Huallaga population. Individuals within the same time points were sampled from different family groups (Table 1).Individually barcoded samples were pooled and sequenced using 50 bp paired end reads on three lanes of the Illumina HiSeq 2500 at the New York Genome Center. This yielded on average 24.45M reads per library ± 8.6M sd (range: 10.1-64.M).

Ranitomeya fantastica and *Ranitomeya variabilis*:

We set up a captive colony consisting of between 6 and 10 wild collected individuals per locality, which was maintained at the Tarapoto Research Center (INIBICO. jr. Ventanilla s/n Sector Ventanilla. Banda de Shilcayo. San Martin, Peru). Male-female pairs were placed into individual terrariums which were misted with rainwater and fed with fruit flies daily. Artificial egg deposition sites consisting of short sections of PVC pipe (~10 cm in length) were positioned within each terrarium and we checked terraria for eggs biweekly. When eggs were found, they were transferred into petri dishes to monitor their development. Upon hatching, tadpoles were placed individually into 25 ml plastic cups filled with rain water and fed daily with a pinch of a 50/50 mix of spirulina and nettle leaf powder. Three tadpoles per stage (7, 14, 35, 49 and 56 days after hatching) were fixed in an RNAlater (Ambion) solution. To do so, tadpoles were first euthanized in a 250 mg/L benzocaine hydrochloride bath, then rinsed with distilled water before the whole tadpole was placed in RNAlater in a 2.5ml Eppendorf tube. The Eppendorf tube with sample in RNAlater was then stored at 4°C for 6h before being frozen at -20°C for long-term storage. This protocol was approved by the Peruvian Servicio Forestal y de Fauna Silvestre through the authorization number 232-2016- SERFOR/DGGSPFFS.

Species	Morph	Age (weeks)	n
Ranitomeya imitator	Redheaded	2	2
		4	2
		7	2
		8	2
	White-Banded	2	3
		4	3
		7	3
		8	3
	Spotted	2	4
		4	4
		7	4
		8	1
	Striped	2	3
		4	3
		7	3
		8	3
Ranitomeya fantastica	Redheaded	1	3
		2	3
		4	3
		5	3
		7	3

		8	3
	White-Banded	4	3
		5	3
		7	3
		8	3
Ranitomeya variabilis	Spotted	1	3
		2	3
		4	3
		5	3
		7	3
		8	3
		9	3
	Striped	1	3
		2	3
		4	3
		5	3
		7	3
		8	3

Supplemental Table 1. Sample sizes for gene expression of model species *R. fantastica* and *R. variabilis.*

SUPPLEMENTAL RESULTS:

Genome sequence data:

We produced a large set of sequence data. This includes approximately 228,115,533,900 10X bases, 22,076,177,973 Oxford Nanopore bases, and 297,076,730,441 PacBio bases.

1323